

A finite element method for modelling electromechanical wave propagation in anisotropic piezoelectric media

S. Rahman^{1,*}, H. P. Langtangen², and C. H. W. Barnes¹

¹*Cavendish Laboratory, Cambridge University, J J Thomson Avenue, Cambridge, CB3 0HE, United Kingdom and*

²*Simula Research Laboratory, Martin Linges v 17, Fornebu P.O.Box 134, 1325 Lysaker, Norway*

We describe and evaluate a numerical solution strategy for simulating surface acoustic waves (SAWs) through semiconductor devices with complex geometries. This multi-physics problem is of particular relevance to the design of SAW-based quantum electronic devices. The mathematical model consists of two coupled partial differential equations for the elastic wave propagation and the electric field, respectively, in anisotropic piezoelectric media. These equations are discretized by the finite element method in space and by a finite difference method in time. The latter method yields a convenient numerical decoupling of the governing equations. We describe how a computer implementation can utilize the decoupling and, via object-oriented programming techniques reuse independent codes for the Poisson equation and the linear time-dependent elasticity equation. First we apply the simulator to a simplified model problem for verifying the implementation, and thereafter we show that the methodology is capable of simulating a real-world case from nanotechnology, involving SAWs in a geometrically non-trivial device made of Gallium Arsenide.

PACS numbers: 02.70.Dc, 85.35.Gv, 73.23.-b, 77.65.Dq, 02.60.x

I. INTRODUCTION

In the process of designing quantum electronic devices based on surface acoustic waves (SAWs) traversing piezoelectric media, it is necessary to determine the effect, on these waves of obstacles such as electrical gates on the surface, and also the effect of the SAW on the low-dimensional quantum mechanical systems such as quantum wires and quantum dots. In general, the gates have a non-trivial geometry, which necessitate numerical simulation tools. The finite element method is well suited to handle complex geometries and is widely used to model piezoelectric devices [1, 2, 3, 4, 5, 6]. The effect on the low-dimensional quantum mechanical systems would be analyzed through coupling the SAW simulator to both stationary and time-dependent Schrödinger equations [7]. This would require the development of a fast SAW simulator but also flexible and portable code.

SAWs are modes of propagation of energy along the free surface of a material such that there is no decay along the direction of propagation but there is exponential decay into the bulk. SAWs have been used in electrical sensor technologies for many decades and have also been a useful tool in probing quantum electronic structures, for example, quantum Hall liquids [8]. Recently, much experimental work has been done in the field of acoustic charge transport whereby a SAW across a GaAs/AlGaAs heterostructure is used to capture a single electron and then transport it along a one-dimensional quantum wire [9]. This would be useful in developing an accurate cur-

rent standard, but more challenging proposals to use this in the burgeoning field of quantum information processing have been proposed [10, 11, 12, 13, 14]. SAWs have also been utilized for both static quantum dot [15] and photo-luminescence experiments [16, 17]. The time and resources required to build such devices are immense, and therefore the mathematical modelling of these devices before the physical construction is advantageous. This approach requires the solution of the continuum electromechanical equations of motion in a piezoelectric medium. The method of partial waves [18] can be used to obtain simple analytical expressions for the waves in the bulk material, but the solutions say nothing about the effect of gates on the surface. Attempts to solve the governing equations analytically for devices which do have surface gates [19, 20, 21] involve simplifications, and the accuracy of these approximations remains uncertain.

There is a vast amount of literature on the three-dimensional finite element analysis of piezoelectric devices [1, 2, 3, 4, 5, 6], and these methods are exploited in the field of ultrasonics to design control systems involving piezoelectric actuators and sensors [22]. Commercial software such as ANSYS and ABAQUS can be used to simulate electromechanical phenomena but lack the flexibility to couple to quantum mechanical calculations such as iterative Poisson-Schrödinger [7]. Therefore it is often necessary to develop one's own computer code for modelling such devices.

In this paper, we formulate and evaluate a finite element based solution method for the equations governing SAWs in piezoelectric media, and we formulate it in a flexible and portable manner to allow the ability to interface with other code. The implementation is performed in an object-oriented style in order to incorporate existing solvers and to enhance portability of the code. Such a tool can be valuable in the design of micro- and nano-scale devices. We describe a set of boundary conditions

*Electronic address: S.Rahman.00@cantab.net

that are capable of efficiently exciting SAWs and demonstrate the propagation of SAWs through a GaAs-based device. Although our applications are specific to GaAs, the formulation is general enough to allow simulations, with the same code (or with small modifications), of any crystal structure provided the elastic and piezoelectric material parameters are known.

This paper is organized as follows. In Section II we give an overview of the mathematical model underlying piezoelectricity and precisely state the coupled partial differential equations we aim to solve. Sections III and IV concern finite element formulations of these equations and an overview of the computational algorithm is described. In section V we describe the class based simulator approach used in our code design which simplifies implementation and increases reliability. Section VI presents a verification of the implementation and an empirical estimation of convergence properties of the numerical solution method. A real-world application of the methodology, concerning a SAW problem in nanotechnology is the subject of Section VII, before we make some concluding remarks in the final section.

II. MODELLING OF PIEZOELECTRIC MATERIALS

For piezoelectric materials, the electric displacement depends on both the applied electric field and mechanical strain, and the stresses depend on both the applied mechanical strain and applied electric field. The electric displacement D_i is given by

$$D_i = \epsilon_{ij}^S E_j + e_{ijk} \varepsilon_{jk}, \quad (1)$$

where E_j denotes the electric field, ϵ_{ij} is the permittivity tensor, e_{ijk} is the piezoelectric coupling constant, ε_{ij} is the strain tensor. The stress tensor σ_{ij} is given by

$$\sigma_{ij} = -e_{kij} E_k + c_{ijkl}^E \varepsilon_{kl}, \quad (2)$$

where c_{ijkl} represents the 4th rank tensor of elastic parameters. Summation over repeated indices is implied in this section, and the superscripts S and E denote that the quantities were measured under constant strain and constant electric field, respectively.

In the absence of free charges within the material, Gauss's law requires the divergence of the electric displacement to vanish:

$$\nabla \cdot D = \varrho_{\text{free}} = 0. \quad (3)$$

Combining Eqs. (1) and (2), and the relation

$$E_i = -\frac{\partial \phi}{\partial x_i} \quad (4)$$

between the electric potential ϕ and the electric field E_i , together with the strain-displacement relation for small strains,

$$\varepsilon_{ij} = \frac{1}{2} \left(\frac{\partial u_j}{\partial x_i} + \frac{\partial u_i}{\partial x_j} \right), \quad (5)$$

where u_i is the mechanical displacement field, we can derive a scalar partial differential equation for ϕ :

$$\frac{\partial}{\partial x_i} \epsilon_{ik}^S \frac{\partial \phi}{\partial x_k} = \frac{\partial}{\partial x_i} e_{ikl} \frac{\partial u_l}{\partial x_k}. \quad (6)$$

This equation couples the potential ϕ and the displacements u_i in the medium, and can be used to compute the electric field. Equation (4) assumes the quasi-static approximation, which requires that very little energy is carried away by electromagnetic waves.

The displacement field in the medium is governed by Newton's 2nd law of motion combined with the appropriate constitutive law. The former equation reads

$$\varrho \ddot{u}_i = \frac{\partial \sigma_{ij}}{\partial x_j} + \varrho b_i, \quad (7)$$

where b_i denotes body forces, and the double dot in \ddot{u}_i denotes a second-order partial derivative in time. As Eq. (7) stands, it contains no damping term, which is irrelevant in our application setting. The constitutive law stated in Eq. (2) relates the stress tensor σ_{ij} to the strain tensor ε_{ij} , and Eq. (5) relates ε_{ij} to the displacement field u_i . Combining Eqs. (2), (5), (7), we arrive at an equation for u_i in terms of ϕ :

$$\varrho \ddot{u}_i = \frac{\partial}{\partial x_j} c_{ijkl}^E \frac{\partial u_l}{\partial x_k} + \varrho b_i + \frac{\partial}{\partial x_j} e_{kij} \frac{\partial \phi}{\partial x_k}. \quad (8)$$

From Eq. (8) we see how the mechanical motion is affected the electric field. In most materials, this coupling is weak, because $e_{ijk} \ll c_{ijkl}^E$, and the effect of the piezoelectric potential on the mechanical deformation is negligible. On the other hand, the effect of the mechanical deformation on the potential is always significant according to Eq. (6). However, in cases where an external electric field is applied through surface gates, the term in ϕ may be sufficiently large to contribute significantly to the mechanical motion, and these cases receive the focus of the present paper.

To illustrate the nature of these equations we explicitly write out the coupling terms for the piezoelectric material GaAs. The elastic parameters of a crystal are usually given in a coordinate system with its x , y and z axes parallel to the crystal X, Y and Z axes. For consistency with acoustoelectric charge transport experiments, we align the positive x axis with the crystal positive [011] axes, and the positive z axis with the crystal positive [100] axis. To achieve this we perform a 45 degree rotation of the crystal, around the z axis.

In the transformed frame, the only non-zero components of the piezoelectric tensor are $e_{15} = -e_{24} = e_{31} = -e_{32}$. For generality, we illustrate our method using the different values of the piezoelectric tensor. Using the as-

sumptions stated in the previous paragraph, and neglecting body forces, we can write out equations Eqs. (8) and (6) as

$$\rho \ddot{u}_x = \frac{\partial}{\partial x_j} c_{xjkl}^E \frac{\partial u_l}{\partial x_k} + \frac{\partial}{\partial x} e_{31} \frac{\partial \phi}{\partial z} + \frac{\partial}{\partial z} e_{15} \frac{\partial \phi}{\partial x}, \quad (9)$$

$$\rho \ddot{u}_y = \frac{\partial}{\partial x_j} c_{yjkl}^E \frac{\partial u_l}{\partial x_k} + \frac{\partial}{\partial y} e_{32} \frac{\partial \phi}{\partial z} + \frac{\partial}{\partial z} e_{24} \frac{\partial \phi}{\partial y}, \quad (10)$$

$$\rho \ddot{u}_z = \frac{\partial}{\partial x_j} c_{zjkl}^E \frac{\partial u_l}{\partial x_k} + \frac{\partial}{\partial x} e_{15} \frac{\partial \phi}{\partial x} + \frac{\partial}{\partial y} e_{24} \frac{\partial \phi}{\partial y}, \quad (11)$$

$$\nabla \cdot \epsilon_s^S \nabla \phi = \frac{\partial}{\partial x} e_{15} \frac{\partial u_z}{\partial x} + \frac{\partial}{\partial y} e_{24} \frac{\partial u_z}{\partial y} + \frac{\partial}{\partial z} e_{31} \frac{\partial u_x}{\partial x} + \frac{\partial}{\partial x} e_{15} \frac{\partial u_x}{\partial z} + \frac{\partial}{\partial z} e_{32} \frac{\partial u_y}{\partial y} + \frac{\partial}{\partial y} e_{24} \frac{\partial u_y}{\partial z}. \quad (12)$$

In Refs. (20) and (21) analytical solutions of these equations were obtained, under the assumption that the ϕ term in Eqs. (9)–(11) can be ignored. This means that the mechanical motion is decoupled from the electric field, but an electric field is induced from the mechanical motion. The reliability of such substantial simplifications

is limited to cases where the external potential ϕ is small. Also, the obtained solutions are for two-dimensional cases only and are therefore of minor interest when studying the effect of surface gates. Solving the fully coupled system of PDEs demands numerical techniques like the one described in the next section.

III. FINITE ELEMENT FORMULATION

We shall use the finite element method in space and the finite difference method in time. The reasons for applying the finite element method are the need for handling geometrically complicated domains and the fact that the method works very well for elasticity problems without coupling to ϕ as well as for the Poisson equation for ϕ .

We point out that the finite element formulation presented in this paper is independent of the choice of element shape, as this would be problem dependent. The elasticity part of the problem has three degrees of freedom - one for each component of the displacement vector. The electrical part has one degree of freedom for the electric potential.

A. The Poisson equation with piezoelectric coupling

Before continuing further, it is convenient to introduce a superscript ℓ to denote the time level, for example, ϕ^ℓ is ϕ at time level ℓ . The electrostatic potential ϕ^ℓ due to mechanical displacements u_i^ℓ in the piezoelectric material concerned is given by Eq. (12). The finite element formulation of such a Poisson equation is well covered in the literature [7, 23, 24, 25]. The basic idea is to approximate ϕ^ℓ by a linear combination of basis functions N_i , $\phi^\ell \approx \hat{\phi}^\ell = \sum_{j=1}^n N_j \phi_j^\ell$, insert $\hat{\phi}^\ell$ in the Poisson equation, and demand the residual to be orthogonal to the space spanned by $\{N_1, \dots, N_n\}$. The Laplace term is integrated by parts.

The only non-trivial aspect of the formulation in the present setting is the right-hand side, where the second-order derivatives of the elastic field demand integration by parts. The two first terms on the right-hand side of Eq. (12) give rise to an integral, which is straightforwardly integrated as

$$\begin{aligned} & - \int_{\Omega} N_i \left[\frac{\partial}{\partial x} e_{15} \frac{\partial u_z^\ell}{\partial x} + \frac{\partial}{\partial y} e_{24} \frac{\partial u_z^\ell}{\partial y} \right] d\Omega \\ & = \int_{\Omega} \left[e_{15} \frac{\partial N_i}{\partial x} \frac{\partial u_z^\ell}{\partial x} + e_{24} \frac{\partial N_i}{\partial y} \frac{\partial u_z^\ell}{\partial y} \right] d\Omega - \oint_{\partial\Omega} N_i \left[e_{15} \frac{\partial u_z^\ell}{\partial x} n_x + e_{24} \frac{\partial u_z^\ell}{\partial y} n_y \right] d\Gamma. \end{aligned} \quad (13)$$

The terms in Eq. (12), containing mixed derivatives, can be integrated by parts using a special form of Green's Theorem,

$$-\int_{\Omega} \phi \frac{\partial \psi}{\partial z} dx dy dz = \int_{\Omega} \frac{\partial \phi}{\partial z} \psi dx dy dz - \oint_{\Gamma} \phi \psi n_z d\Gamma. \quad (14)$$

The terms give rise to the integrals

$$\begin{aligned} & -\int_{\Omega} N_i \left[\frac{\partial}{\partial z} e_{31} \frac{\partial u_x^\ell}{\partial x} + \frac{\partial}{\partial x} e_{15} \frac{\partial u_x^\ell}{\partial z} + \frac{\partial}{\partial z} e_{32} \frac{\partial u_y^\ell}{\partial y} + \frac{\partial}{\partial y} e_{24} \frac{\partial u_y^\ell}{\partial z} \right] d\Omega \\ & = \int_{\Omega} \left[e_{31} \frac{\partial N_i}{\partial z} \frac{\partial u_x^\ell}{\partial x} + e_{15} \frac{\partial N_i}{\partial x} \frac{\partial u_x^\ell}{\partial z} + e_{32} \frac{\partial N_i}{\partial z} \frac{\partial u_y^\ell}{\partial y} + e_{24} \frac{\partial N_i}{\partial y} \frac{\partial u_y^\ell}{\partial z} \right] d\Omega \\ & - \oint_{\partial\Omega} N_i \left[e_{31} \frac{\partial u_x^\ell}{\partial x} n_z + e_{15} \frac{\partial u_x^\ell}{\partial z} n_x + e_{32} \frac{\partial u_y^\ell}{\partial y} n_z + e_{24} \frac{\partial u_y^\ell}{\partial z} n_y \right] d\Gamma. \end{aligned} \quad (15)$$

The finite element method applied to the equation for ϕ transforms the PDE problem to a linear system of equations,

$$\mathbf{P}\boldsymbol{\phi}^\ell = \mathbf{f}^\ell, \quad (16)$$

where the ‘stiffness’ matrix \mathbf{P} has its (i, j) element given by

$$P_{ij} = \int_{\Omega} \epsilon_s^S \left[\frac{\partial N_i}{\partial x} \frac{\partial N_j}{\partial x} + \frac{\partial N_i}{\partial y} \frac{\partial N_j}{\partial y} + \frac{\partial N_i}{\partial z} \frac{\partial N_j}{\partial z} \right] d\Omega. \quad (17)$$

The $\boldsymbol{\phi}^\ell$ vector in Eq. (16) contains the values of ϕ^ℓ at the nodal points. The i -th component f_i^ℓ of the right-hand side vector \mathbf{f}^ℓ can be written as

$$f_i^\ell = \oint_{\partial\Omega} \epsilon_s^S N_i \frac{\partial \phi^\ell}{\partial n} d\Gamma - \oint_{\partial\Omega} N_i r d\Gamma + \int_{\Omega} s d\Omega, \quad (18)$$

with

$$\begin{aligned} r &= e_{31} \frac{\partial u_x^\ell}{\partial x} n_z + e_{15} \frac{\partial u_x^\ell}{\partial z} n_x + e_{32} \frac{\partial u_y^\ell}{\partial y} n_z + e_{24} \frac{\partial u_y^\ell}{\partial z} n_y + e_{15} \frac{\partial u_z^\ell}{\partial x} n_x + e_{24} \frac{\partial u_z^\ell}{\partial y} n_y, \\ s &= e_{31} \frac{\partial N_i}{\partial z} \frac{\partial u_x^\ell}{\partial x} + e_{15} \frac{\partial N_i}{\partial x} \frac{\partial u_x^\ell}{\partial z} + e_{32} \frac{\partial N_i}{\partial z} \frac{\partial u_y^\ell}{\partial y} + e_{24} \frac{\partial N_i}{\partial y} \frac{\partial u_y^\ell}{\partial z} + e_{15} \frac{\partial N_i}{\partial x} \frac{\partial u_z^\ell}{\partial x} + e_{24} \frac{\partial N_i}{\partial y} \frac{\partial u_z^\ell}{\partial y}. \end{aligned}$$

When the displacement field entering f_i^ℓ is known, any standard Poisson solver can be used to compute $\boldsymbol{\phi}^\ell$.

B. The elasticity problem with electric field loading

For the finite element formulation of Eq. (8) it is easier to first start with Eq. (7) and insert the constitutive law given by Eq. (2) and the strain-displacement relation given by Eq. (5) in the finite element integrals. The time derivative in Eq. (8) can be approximated by a second-order accurate finite difference. Sampling Eq. (8) at time level ℓ then yields

$$\varrho \frac{u_i^{\ell-1} - 2u_i^\ell + u_i^{\ell+1}}{\Delta t^2} = \frac{\partial \sigma_{ij}^\ell}{\partial x_j} + \varrho b_i^\ell, \quad (19)$$

where Δt is the time step length and quantities with the ℓ superscript are functions of space only. This time discretization introduces an operator splitting such that the originally coupled governing equations can be solved in

sequence. No accuracy is lost by this operator splitting beyond that implied by the finite difference itself in Eq. (19). More precisely, σ_{ij}^ℓ contains ϕ^ℓ , which is known, such that we can easily solve for $u_i^{\ell+1}$ using old values of ϕ . On the next time level $(\ell + 1)$, we can find $\phi^{\ell+1}$ using the recently computed $u_i^{\ell+1}$.

The main motivation for the explicit time differencing in Eq. (19) is numerical efficiency: (i) we decouple the equations, which simplifies the numerics and the implementation, and (ii) there is no need to solve large sparse linear systems of equations in the elasticity part of the problem (if the mass matrix is lumped). Nevertheless, the time difference Eq. (19) leads to a conditionally stable scheme, where Δt must be of the order of the smallest element size. In wave propagation problems, uniform high resolution is frequently needed in space and time, typically compatible with the stability restriction, which makes such explicit schemes appropriate. On the other hand, in applications where adaptive grids with great variation in element size are needed, one may benefit from implicit schemes (for example, of Newmark type) [24].

The finite element formulation of Eq. (19) is easiest to express if we switch to a typical “finite element engineering” notation, especially when we deal with anisotropic media. The stress and strain tensors are expressed as vectors,

$$\begin{aligned}\boldsymbol{\sigma} &= (\sigma_{xx}, \sigma_{yy}, \sigma_{zz}, \sigma_{yz}, \sigma_{zx}, \sigma_{yx})^T, \\ \boldsymbol{\varepsilon} &= (\varepsilon_{xx}, \varepsilon_{yy}, \varepsilon_{zz}, 2\varepsilon_{yz}, 2\varepsilon_{zx}, 2\varepsilon_{yx})^T.\end{aligned}$$

The constitutive law can then be written as

$$\boldsymbol{\sigma}^\ell = \mathbf{D}\boldsymbol{\varepsilon}^\ell + \mathbf{p}^\ell, \quad (20)$$

where the \mathbf{p}^ℓ term represents the loading from the electric field, and \mathbf{D} is a symmetric 6×6 matrix of the elasticity coefficients (previously denoted by c_{ijkl}^E):

$$\mathbf{D} = \begin{bmatrix} c_{11} & c_{12} & c_{13} & c_{14} & c_{15} & c_{16} \\ & c_{12} & c_{13} & c_{14} & c_{15} & c_{16} \\ & & c_{13} & c_{14} & c_{15} & c_{16} \\ & & & c_{14} & c_{15} & c_{16} \\ & & & & c_{15} & c_{16} \\ & & & & & c_{16} \end{bmatrix}. \quad (21)$$

The displacement field at a time level ℓ is approximated according to

$$u_i^\ell \approx \hat{\mathbf{u}}^\ell = \sum_{j=1}^n N_j \mathbf{u}_j^\ell,$$

where \mathbf{u}_j^ℓ is the value of the displacement field at node j at time level ℓ . The strain-displacement relation then becomes

$$\boldsymbol{\varepsilon}^\ell = \sum_{j=1}^n \mathbf{B}_j \mathbf{u}_j^\ell, \quad \mathbf{B}_i = \begin{bmatrix} N_{i,x} & 0 & 0 \\ 0 & N_{i,y} & 0 \\ 0 & 0 & N_{i,z} \\ 0 & N_{i,z} & N_{i,y} \\ N_{i,z} & 0 & N_{i,x} \\ N_{i,y} & N_{i,x} & 0 \end{bmatrix}. \quad (22)$$

The comma notation here denotes partial derivative: $N_{i,x} \equiv \partial N_i / \partial x$.

A finite element formulation of Eq. (19) using the aforementioned notation becomes (see Ref. 23 for a detailed derivation without the ϕ term)

$$\int_{\Omega} \varrho N_i \sum_{j=1}^n N_j (\mathbf{u}_j^{\ell-1} - 2\mathbf{u}_j^\ell + \mathbf{u}_j^{\ell+1}) d\Omega + \Delta t^2 \int_{\Omega} \mathbf{B}_i^T \boldsymbol{\sigma}^\ell d\Omega = \Delta t^2 \int_{\Omega} \varrho \mathbf{b} N_i d\Omega + \Delta t^2 \int_{\partial\Omega} \mathbf{t}^\ell N_i d\Gamma. \quad (23)$$

Here, \mathbf{t}^ℓ is the traction on the boundary, arising from integrating the divergence of the stress in Eq. (19) by parts. Inserting the constitutive law in the term $\int_{\Omega} \mathbf{B}_i^T \boldsymbol{\sigma} d\Omega$ yields

$$\sum_{j=1}^n \left(\int_{\Omega} \mathbf{B}_i^T D \mathbf{B}_j d\Omega \right) \mathbf{u}_j^\ell + \int_{\Omega} \mathbf{B}_i^T \mathbf{p}^\ell d\Omega.$$

The final discrete equations arising from the equation of motion can be written as

$$\mathbf{u}^{\ell+1} = 2\mathbf{u}^\ell - \mathbf{u}^{\ell-1} + \Delta t^2 \tilde{\mathbf{M}}^{-1} (-\mathbf{K} \mathbf{u}^\ell + \boldsymbol{\beta}^\ell + \boldsymbol{\Phi}^\ell), \quad (24)$$

where $\tilde{\mathbf{M}}^{-1}$ is an efficient inverse of the mass matrix \mathbf{M} resulting from the $\int_{\Omega} \rho N_i N_j d\Omega$ integral. We construct $\tilde{\mathbf{M}}^{-1}$ as the inverse of the lumped mass matrix (using the row-sum technique to lump the matrix). The matrix \mathbf{K} stems from the standard “stiffness” term $\int_{\Omega} \mathbf{B}_i^T D \mathbf{B}_j d\Omega$ representing anisotropic elasticity, $\boldsymbol{\beta}^\ell$ is the effect of body forces and surface tractions, and $\boldsymbol{\Phi}^\ell$ is the contribution from the electric field. The i -th block (arising from node i) in $\boldsymbol{\Phi}^\ell$ takes the form $\boldsymbol{\Phi}_i^\ell = \int_{\Omega} \mathbf{B}_i^T \mathbf{p}^\ell$, which from Eqs. (9) to (11) results in

$$\boldsymbol{\Phi}_i^\ell = \begin{bmatrix} \int_{\Omega} N_i \left[\frac{\partial}{\partial x} e_{31} \frac{\partial \phi^\ell}{\partial z} + \frac{\partial}{\partial z} e_{15} \frac{\partial \phi^\ell}{\partial x} \right] d\Omega \\ - \int_{\Omega} N_i \left[\frac{\partial}{\partial y} e_{32} \frac{\partial \phi^\ell}{\partial z} + \frac{\partial}{\partial z} e_{24} \frac{\partial \phi^\ell}{\partial y} \right] d\Omega \\ \int_{\Omega} N_i \left[\frac{\partial}{\partial x} e_{15} \frac{\partial \phi^\ell}{\partial x} + \frac{\partial}{\partial y} e_{24} \frac{\partial \phi^\ell}{\partial y} \right] d\Omega \end{bmatrix}$$

$$= \begin{bmatrix} - \int_{\Omega} \left[e_{31} \frac{\partial N_i}{\partial x} \frac{\partial \phi^\ell}{\partial z} + e_{15} \frac{\partial N_i}{\partial z} \frac{\partial \phi^\ell}{\partial x} \right] d\Omega + \int_{\partial\Omega} N_i \left[e_{31} \frac{\partial \phi^\ell}{\partial z} n_x + e_{15} \frac{\partial \phi^\ell}{\partial x} n_z \right] d\Gamma \\ \int_{\Omega} \left[e_{32} \frac{\partial N_i}{\partial y} \frac{\partial \phi^\ell}{\partial z} + e_{24} \frac{\partial N_i}{\partial z} \frac{\partial \phi^\ell}{\partial y} \right] d\Omega - \int_{\partial\Omega} N_i \left[e_{32} \frac{\partial \phi^\ell}{\partial z} n_y + e_{24} \frac{\partial \phi^\ell}{\partial y} n_z \right] d\Gamma \\ - \int_{\Omega} \left[e_{15} \frac{\partial N_i}{\partial x} \frac{\partial \phi^\ell}{\partial x} + e_{24} \frac{\partial N_i}{\partial y} \frac{\partial \phi^\ell}{\partial y} \right] d\Omega + \int_{\partial\Omega} N_i \left[e_{15} \frac{\partial \phi^\ell}{\partial x} n_x + e_{24} \frac{\partial \phi^\ell}{\partial y} n_y \right] d\Gamma \end{bmatrix}. \quad (25)$$

Our governing equations require initial conditions. Let us assume that the elastic body is at rest such that $\partial u_i / \partial t = 0$. The external electric field is then turned on. After the initial transients the displacement field have faded out, and we have a stationary initial state of our system, modeled by the equations

$$\mathbf{P} \boldsymbol{\phi}^0 = \mathbf{f}^0(\mathbf{u}^0), \quad (26)$$

$$\mathbf{K} \mathbf{u}^0 = \boldsymbol{\beta}^0 + \boldsymbol{\Phi}^0(\boldsymbol{\phi}^0). \quad (27)$$

These two coupled equations are solved by an iterative Gauss-Seidel-like technique, i.e., the equations are solved one at a time, using the most recent approximation of the other field in the right-hand side term. Each linear system is solved by a MILU preconditioned conjugate gradient method [26]. The solution of Eqs. (26) and (27), along with the assumption of stationarity, $\partial \mathbf{u} / \partial t = 0$, comprise the initial condition.

As boundary conditions, we either have prescribed traction components or prescribed displacement components, along with prescribed electric potential or prescribed normal component of the electric field. The displacement equation needs three boundary conditions at each point at the boundary, while the equation for ϕ needs one condition at each point.

From $\partial \mathbf{u} / \partial t = 0$ at $t = 0$ it follows by a second-order difference approximation that $\mathbf{u}^1 = \mathbf{u}^{-1}$. From Eqs. (24) and (27) it follows that $\mathbf{u}^1 = \mathbf{u}^0 = \mathbf{u}^{-1}$. The loads removed at $t = 0^+$ will first come into play at the second time level.

The computational algorithm can now be formulated as follows:

$\ell = 0$ (time level counter)
 $k = 0$ (iteration counter)
 while $\varepsilon < \varepsilon_{crit}$
 solve Eq. (26) w.r.t $\boldsymbol{\phi}^{0,k}$

solve Eq. (27) w.r.t $\mathbf{u}^{0,k}$
 compute $\varepsilon = \|\mathbf{u}^{0,k} - \mathbf{u}^{0,k-1}\| + \|\phi^{0,k} - \phi^{0,k-1}\|$
 $k \leftarrow k + 1$ end while
 $\phi^1 = \phi^0, \mathbf{u}^1 = \mathbf{u}^0$
 for $\ell = 1, 2, 3, \dots$ until end of simulation
 solve Eq. (24) w.r.t $\mathbf{u}^{\ell+1}$
 solve Eq. (16) w.r.t $\phi^{\ell+1}$

Comments on Stability. The stability criterion of the explicit finite difference scheme in time, when decoupled from the electric field problem, requires $\Delta t \leq 2/\omega_{\max}$ [27], where ω_{\max} is the highest natural frequency of the vibrating system. One may find ω_{\max} as the square root of the largest eigenvalue of the problem $\mathbf{K} - \lambda\mathbf{M} = 0$. An approximate bound on ω_{\max} can be estimated from a relation $\omega_{\max} = 2c/h_{\text{eff}}$, where c is the speed of elastic waves and h_{eff} is the smallest effective element length. The stability criterion now reduces to the common Courant, Friedrichs, and Lewy (CFL) condition:

$$\Delta t \leq \alpha h_{\text{eff}}/c. \quad (28)$$

Here, α is a factor to be adjusted since the h_{eff} parameter is normally roughly computed from element sizes or application of Gerschgorin's theorem applied to the underlying eigenvalue problem. For wave problems the CFL condition is frequently not particularly restrictive since the length and period of a wave are usually proportional, leading to a natural choice of $\Delta t/h = \text{const.}$

IV. AN OPTIMISED FINITE ELEMENT FORMULATION

We can speed up the numerical computation by replacing the complete assembly of the right-hand side vectors in Eqs. (16) and (24) by a matrix-vector product. For example, consider the contribution to the vector \mathbf{f} in Eq. (16) due to the coupling from the mechanical motion (omitting the superscript ℓ for the remainder of this section):

$$\int_{\Omega} e_{31} \frac{\partial N_i}{\partial z} \frac{\partial u_x}{\partial x} + e_{15} \frac{\partial N_i}{\partial x} \frac{\partial u_x}{\partial z} + e_{32} \frac{\partial N_i}{\partial z} \frac{\partial u_y}{\partial y} + e_{24} \frac{\partial N_i}{\partial y} \frac{\partial u_y}{\partial z} + e_{15} \frac{\partial N_i}{\partial x} \frac{\partial u_z}{\partial x} + e_{24} \frac{\partial N_i}{\partial y} \frac{\partial u_z}{\partial y} d\Omega. \quad (29)$$

Inserting the finite element expansion $u_x \approx \sum_{j=1}^n u_j^{(x)} N_j$, and similar expansions for u_y and u_z , the expression in Eq. (29) results in

$$\begin{aligned} \sum_{j=1}^n \int_{\Omega} & e_{31} \frac{\partial N_i}{\partial z} \frac{\partial N_j}{\partial x} u_j^{(x)} + e_{15} \frac{\partial N_i}{\partial x} \frac{\partial N_j}{\partial z} u_j^{(x)} + e_{32} \frac{\partial N_i}{\partial z} \frac{\partial N_j}{\partial y} u_j^{(y)} \\ & + e_{24} \frac{\partial N_i}{\partial y} \frac{\partial N_j}{\partial z} u_j^{(y)} + e_{15} \frac{\partial N_i}{\partial x} \frac{\partial N_j}{\partial x} u_j^{(z)} + e_{24} \frac{\partial N_i}{\partial y} \frac{\partial N_j}{\partial y} u_j^{(z)} d\Omega. \end{aligned} \quad (30)$$

This expression can be written as a matrix vector product $\mathbf{L}\mathbf{u}$, where the matrix \mathbf{L} consists of $n \times n$ blocks, each block of size 1×3 . For the coupling of node i and j , the 3×1 block looks like

$$e_{31} \frac{\partial N_i}{\partial z} \frac{\partial N_j}{\partial x} + e_{15} \frac{\partial N_i}{\partial x} \frac{\partial N_j}{\partial z}, e_{32} \frac{\partial N_i}{\partial z} \frac{\partial N_j}{\partial y} + e_{24} \frac{\partial N_i}{\partial y} \frac{\partial N_j}{\partial z}, e_{15} \frac{\partial N_i}{\partial x} \frac{\partial N_j}{\partial x} + e_{24} \frac{\partial N_i}{\partial y} \frac{\partial N_j}{\partial y}, \quad (31)$$

The Poisson equation - Eq. (16) for ϕ can now be written as

$$\mathbf{P}\phi^{\ell+1} = \mathbf{L}\mathbf{u}^{\ell+1}. \quad (32)$$

At each time level we can hence avoid the costly finite element assembly process, since \mathbf{P} and \mathbf{L} are constant in time and the right-hand side of the linear system is obtained by an efficient matrix-vector product. This may result in a significant speed-up of the solver. For large number of unknowns, the speed up is experienced only if we use a method of complexity or order n , like multigrid, to solve Eq. (32).

Equation (24) is already on a favorable matrix-vector algebra form, except for the coupling term Φ^ℓ . Examining Eq. (25), we realize that this matrix can be written as $\Phi^\ell = \mathbf{Q}\phi^\ell$, where \mathbf{Q} is a time-independent $n \times n$ matrix of 3×1 blocks. The contribution to block i in Φ^ℓ is made of the coupling \mathbf{Q}_{ij} between node i and j and the block j in ϕ^ℓ : $\Phi_i^\ell = \mathbf{Q}_{ij}\phi_j^\ell$, where

$$\mathbf{Q}_{ij} = \begin{bmatrix} -\int_{\Omega} e_{31} \frac{\partial N_i}{\partial x} \frac{\partial N_j}{\partial z} + e_{15} \frac{\partial N_i}{\partial z} \frac{\partial N_j}{\partial x} d\Omega + \int_{\partial\Omega} N_i [e_{31} \frac{\partial N_j}{\partial z} n_x + e_{15} \frac{\partial N_j}{\partial x} n_z] d\Gamma \\ \int_{\Omega} e_{32} \frac{\partial N_i}{\partial y} \frac{\partial N_j}{\partial z} + e_{24} \frac{\partial N_i}{\partial z} \frac{\partial N_j}{\partial y} d\Omega - \int_{\partial\Omega} N_i [e_{32} \frac{\partial N_j}{\partial z} n_y + e_{24} \frac{\partial N_j}{\partial y} n_z] d\Gamma \\ -\int_{\Omega} e_{15} \frac{\partial N_i}{\partial x} \frac{\partial N_j}{\partial x} + e_{24} \frac{\partial N_i}{\partial y} \frac{\partial N_j}{\partial y} d\Omega + \int_{\partial\Omega} N_i [e_{15} \frac{\partial N_j}{\partial x} n_x + e_{24} \frac{\partial N_j}{\partial y} n_y] d\Gamma \end{bmatrix}.$$

Now the Φ^ℓ term in Eq. (24) can be computed as a matrix-vector product $\mathbf{Q}\phi^\ell$, and no assembly process is required to construct Eq. (24) at each time level. In our algorithm we must run assembly processes at $t = 0$ to construct the matrices $\tilde{\mathbf{M}}^{-1}$, \mathbf{K} , \mathbf{Q} , \mathbf{L} , and \mathbf{P} .

V. OBJECT-ORIENTED IMPLEMENTATION

A significant trend in modern software development is to formulate numerical algorithms such that reliable and well-tested software components can be combined together to form a new simulator. Our numerical approach was in particular inspired by such an approach. With the time discretization we were able to split the coupled u_i - ϕ system such that at each time level we first solve for a new displacement field (u_i) and then we solve for the corresponding electric potential (ϕ). In each of the two equations, the effect of the other only enters through a right-hand side “forcing” term. This allows us, in principle, to reuse a solver for elastic vibrations and a Poisson solver, as long as these solvers can implement a new right-hand side term that couples to another solver. From a principal point of view, this idea is simple and attractive. However, the implementation of the idea in practice may be less feasible if the design of the underlying solvers is not sufficiently flexible.

To allow for building the compound u_i - ϕ solver from separate u_i and ϕ solvers we propose to apply principles from object-oriented programming. The time-dependent elasticity solver and the Poisson solver are realized as two independent objects, implemented via classes in C++. Actually, we have reused the `Poisson2` class from Ref. 23 as the Poisson solver, and the `ElasticVib1` class from Ref. 23 as the elastic vibration solver. The latter is a subclass of `Elasticity2`, a pure quasi time-dependent elasticity solver (without the acceleration term in the momentum equation). These classes are implemented using building blocks from the Diffpack library [23].

The `Poisson2` and `ElasticVib1` classes have no knowledge of each other. The only common feature is their design. This design is crucial for reuse of the classes to solve the coupled problem, but the design approach suggested for Diffpack solvers [23, 28, 29] has proven to be successful in this respect. Diffpack solvers are realized as classes containing objects for grids, scalar/vector fields, linear systems, etc. The coefficients in a PDE are

evaluated through virtual functions. When the solver is stand-alone, these virtual functions contain mathematical expressions or measured data, but when solvers are combined, the virtual functions are reimplemented in subclasses and connected to data in other solvers. This principle reflects the underlying mathematics: the coefficients in a single PDE are considered known, but in a system of PDEs, the coefficients typically couple to unknown quantities governed by the PDEs. The present coupled system is an example where the right-hand side in the Poisson equation couples to the primary unknown in the elastic vibration solver, while a right-hand side term in the elastic vibration solver couples to the primary unknown in the Poisson equation. When the solvers are used independently there are no such couplings.

Figure 1 shows an outline of the class design for the compound solver. From class `Poisson2` we derive a subclass `Poisson2_glue`, which reimplements the virtual function in `Poisson2` for evaluating the right-hand side in that equation. In this new function we need to compute an expression involving the displacement field available in the `ElasticVib1` class. A manager class, simply called `Manager`, holds pointers to all classes for the individual PDEs in the system of PDEs, and each PDE class holds a pointer to the manager class, thus enabling a two-way communication. With these pointers, we can connect data from any other solver class to the `Poisson2_glue` class. In the virtual function evaluating the right-hand side we can typically call `mng->elastic->u` to get a vector field object for u_i that we can evaluate at the current integration point. This object has support for evaluating derivatives of the field as well.

Similarly, we derive a subclass `ElasticVib1_glue` of `ElasticVib1`, add a pointer to the manager class, and override the virtual function for evaluating the right-hand side. Now we need to compute expressions involving ϕ , but this is easily accomplished by the pointers, e.g., `mng->poisson->u` if `u` is the name of the unknown scalar field in the `Poisson2` solver.

The “glue” classes `Poisson2_glue` and `ElasticVib1_glue`

are very small compared to the real solver classes they inherit from. A “glue” class typically needs about a page of code unless it adds additional computations. The manager class is a bit more comprehensive since it implements the overall solution algorithm, i.e., the time stepping and the calls to the independent solvers.

The benefit from using object-oriented programming in the way we have outlined is that the original well-tested Poisson and elastic vibration solvers can be reused in a system of PDEs without any modifications. The original solver classes reside in separate files and are hence not subject to any side effects from editing the source code. The “glue” class is also in a separate file and enables the original solver to speak to a manager in charge of solving a compound system of PDEs. The advantages are clear: reliability is increased by reusing well-tested solvers, and the compound solver is modularized. Our experience is that this design reduces the development time significantly. Especially the debugging phase is greatly simplified. At any time, the underlying solvers can be trivially pulled out of the compound system and verified independently.

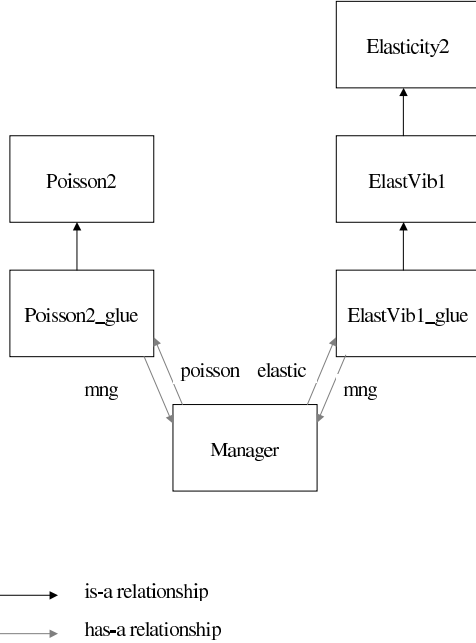


FIG. 1: Relationships between classes. The base classes, `Poisson2` and `Elasticity2` perform the solution of the standard time-independent Poisson and elasticity equations, respectively. `ElasticVib1` is derived from `Elasticity2` and solves for time-dependent elastic motion. The classes `Poisson2_glue` and `ElasticVib1_glue` implement the coupling between the electrostatic and mechanical equations, and these classes are controlled by the `Manager` class.

VI. VERIFICATION

Before showing numerical results for a physically relevant application, we report on the estimated numerical

accuracy of the code, thereby establishing evidence for the correctness of the implementation. To investigate numerical errors, we compare numerical results with an exact solution. The exact solution is based on the assumption of a displacement field in z direction only, depending on x and t only. Physically, a normal traction is applied at all $x = \text{const}$ and $y = \text{const}$ boundaries to avoid displacements in the x and y directions, but in the code we implement this situation by essential boundary conditions $u_x = u_y = 0$. We also assume that $\phi = \phi(x, t)$ and that the material is isotropic. The governing equations then reduce to

$$\varrho \ddot{u}_z = \mu \frac{\partial^2 u_z}{\partial x^2} + e_{15} \frac{\partial^2 \phi}{\partial x^2}, \quad (33)$$

$$\epsilon_s \frac{\partial^2 \phi}{\partial x^2} = e_{15} \frac{\partial^2 u_z}{\partial x^2}. \quad (34)$$

These equations can be scaled to yield

$$\ddot{u}_z = \frac{\partial^2 u_z}{\partial x^2} + \alpha \frac{\partial^2 \phi}{\partial x^2}, \quad (35)$$

$$\frac{\partial^2 \phi}{\partial x^2} = \frac{\partial^2 u_z}{\partial x^2}. \quad (36)$$

The constant α is zero or unity corresponding to whether the elasticity problem couples to the electric field problem or not. (The three coefficients in the original system are scaled away by choosing an appropriate time scale, ϕ scale, and u_i scale.) One possible solution of Eqs. (35)–(36) reads

$$u_z(x, t) = \phi(x, t) = \cos(k\sqrt{1+\alpha}t) \sin(kx). \quad (37)$$

In our tests we choose Ω as a three-dimensional beam and $k = \frac{n\pi}{L}$, with n being an integer and L the length of the beam. The ends of the beam are then fixed.

Our verification procedure consists of estimating the convergence rate of the numerical method. A scalar error measure e is expected to behave like

$$e = Ah^r + B\Delta t^s,$$

where A and B are constants independent of the element size h and the time step Δt . From the involved approximations, we expect $s = 2$ and $r = 1 + q$, where q is the order of the polynomials in an element. In particular, for linear or trilinear elements, $r = 2$, and if h and Δt are chosen such that $h/\Delta t = \text{const}$, we see that $e \sim h^r$. From two successive experiments, (h_{i-1}, e_{i-1}) and (h_i, e_i) we may estimate a convergence rate r_i from

$$r_i = \frac{\ln e_i / e_{i-1}}{\ln h_i / h_{i-1}}.$$

We have investigated three error measures, given as different norms of the error field $E = u_z - \hat{u}_z$, where \hat{u}_z is the numerical solution and u_z is the exact solution:

$$\|E\|_{L^1(\Omega)} = \int_{\Omega} |E| d\Omega, \quad \|E\|_{L^2(\Omega)} = \left(\int_{\Omega} E^2 d\Omega \right)^{\frac{1}{2}}, \quad \|E\|_{L^\infty(\Omega)} = \sup(|E(\mathbf{x})|, \mathbf{x} \in \Omega).$$

Table I displays the values of the error norms and the associated estimates of the convergence rates r_i . As the grid spacing h and the time step Δt are reduced, the numerical solution converges to the exact solution with the expected rate of two. This provides evidence for the correctness of the implementation and indicates that our overall solution method, including the operator splitting, is of second order in time and space. The spatial convergence rate is expected to increase with the order of the polynomials used in the elements.

h	$\ E\ _{L^1}$	rates	$\ E\ _{L^2}$	rates	$\ E\ _{L^\infty}$	rates
0.05	$2.440 \cdot 10^{-5}$		$2.710 \cdot 10^{-6}$		$3.830 \cdot 10^{-7}$	
0.1	$9.760 \cdot 10^{-5}$	1.999	$1.084 \cdot 10^{-6}$	2.000	$1.533 \cdot 10^{-6}$	2.000
0.2	$3.902 \cdot 10^{-4}$	1.999	$4.335 \cdot 10^{-5}$	1.999	$6.130 \cdot 10^{-6}$	1.999
0.25	$6.096 \cdot 10^{-4}$	1.999	$6.771 \cdot 10^{-5}$	1.999	$9.574 \cdot 10^{-6}$	1.999
0.5	$2.432 \cdot 10^{-3}$	1.996	$2.702 \cdot 10^{-4}$	1.996	$3.819 \cdot 10^{-5}$	1.996

TABLE I: Error norms and estimated convergence rates for waves in a piezoelectric material, with $h = 10\Delta t$.

VII. A SURFACE ACOUSTIC WAVE APPLICATION

In order to show that our suggested numerical model may be applied to real-world phenomena, we apply it to a problem in quantum electronics, specifically in acoustic charge transport. We simulate a SAW propagating through a nano-scale substrate of GaAs. SAWs are particular solutions of Eqs. (9) - (12) such that they propagate without decay on the surface of a material but decay exponentially into the bulk. The solutions typically have the form,

$$u_i = \sum_j U_{i,j} e^{-kq_j z} e^{i(kx - \omega t)}, \quad (38)$$

$$\phi = \sum_j \Phi_j e^{-kq_j z} e^{i(kx - \omega t)},$$

assuming x is the direction of propagation, z is the direction into the bulk ($z \rightarrow -\infty$), and the decay constants q_j , may be complex, allowing for oscillatory decay (in an exponential envelope) into the bulk as is the case for GaAs [30]. The $U_{i,j}$ and Φ_j are constant amplitudes, and k is a wavenumber. It is a straightforward mathematical procedure to determine the decay constants and wave velocity [18]. However, we are interested in the more complicated dynamics taking place when an obstacle in the form of a charged metallic gate is placed on the surface.

In acoustic charge transport, the time-varying electric potential accompanying the SAW is used to transport electrons which are trapped in the minima of the waves. To perform further manipulation on these electrons, for example, to remove some from a minimum, external electric fields must be applied, and this is achieved by applying voltages to metallic gates placed on the surface. In general, the gates have different electrical and mechanical properties to the bulk piezoelectric material and so we may expect to see interesting effects if for example a SAW is passed through the compound structure. Here, we perform three simulations where we pass a SAW through a piece of GaAs. The first will be a bare SAW, as a check to see we do excite the required modes. The following two will have a metallic gate of contrasting mechanical properties to GaAs with a static voltage applied on it. In the first of these, we decouple the mechanical motion from the electric field (while keeping the electric field coupled to the mechanical motion). In the second we allow the full mutual coupling between the electrical and mechanical fields to take place. The dimensions of the gate are $600 \text{ nm} \times 400 \text{ nm} \times 200 \text{ nm}$. To magnify the effect of the compound material structure we use a fictitious material for the gate, similar in crystal structure to GaAs, but with the elastic constants and mass density changed by one order of magnitude. Moreover, we apply a relatively large voltage of 1.5 V so that the coupling of the mechanical displacement to the electric field is evident.

In the numerical simulations we have implemented 8-noded hexahedral brick elements with $2 \times 2 \times 2$ Gauss-Legendre integration. The spacing along the direction of the SAW propagation - Δx is chosen to be 100 nm. The time integration parameter Δt is 1.25×10^{-2} ns.

A. Experiments with surface acoustic waves

In realistic SAW-based devices, bulk waves and SAWs are excited by the application of a microwave signal to an interdigitated transducer. The waves propagate outward from the source, with bulk waves dissipating energy into the bulk and surface acoustic waves travelling through the free surface. In acoustoelectric charge transport experiments, the quantum devices are located several thousand microns away from the source where one would expect to see only surface acoustic waves. To simulate the entire system would therefore require vast computational resources (the wavelength of a SAW is one micron and approximately ten nodes would be required across one wavelength for a satisfactory description). Instead we describe a system of boundary conditions which excite acoustic waves with SAWs dominating over the bulk

waves within a few microns of the source.

1. Excitation of SAWs.

We point out that to be consistent with the formulation presented in the previous sections and hence acoustoelectric charge transport experiments, in our simulations the SAW travels along the crystal positive [011] axis, with the positive z axis aligned with the crystal positive [100] axis.

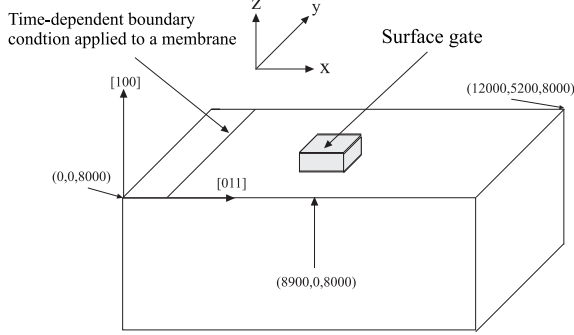


FIG. 2: A schematic diagram of the experimental setup for simulating SAWs. The gate is centered at $(8.9 \cdot 10^3 \text{ nm}, 2.6 \cdot 10^3 \text{ nm})$

In order to excite the SAW modes, we apply a time-dependent Dirichlet boundary condition to the z component of the displacement field on a small region on the grid. This can be expressed as

$$\begin{aligned} u_x = u_y = 0, \quad u_z = A \sin(2\pi ft), \\ x_0 \leq x \leq x_1, \quad z = 8000 \text{ nm}. \end{aligned} \quad (39)$$

The thickness of the membrane is defined as $x_1 - x_0 = 100 \text{ nm}$. To reduce diffraction effects from the surfaces - $y = 0 \text{ nm}$ and $y = 5200 \text{ nm}$ we have forced $u_y = 0$ on those faces. The frequency f used is 2.7 GHz and the amplitude A is chosen so that the SAW amplitude is approximately 20 mV at a depth of 100 nm . Traction free boundary conditions for the mechanical equations and zero normal electrical displacements are implemented at the surfaces. We found this system of boundary conditions to be a particularly efficient means of generating coherent SAWs. The setup is shown in Fig. 2.

Figure 3 is a result of a simulation showing the $\frac{\pi}{2}$ phase difference between the x and z components of the displacement vector, and the larger z amplitude, suggesting elliptical polarization in the sagittal plane. Figures 4(a) and 4(b) show two-dimensional slices, in perpendicular planes, of the full three-dimensional solutions. The first shows the non-decaying nature of these waves along the propagation direction. The SAW wavelength can be seen to be approximately 1000 nm and its velocity is computed to be approximately $2700 \pm 20 \text{ ms}^{-1}$, which is in

good agreement with analytical calculations for the wave velocity. The second figure shows the surface nature of these waves; the greatest amplitude is near the surface and there is no observable decay in the direction of propagation but they decay exponentially into the bulk. On the far left of each image (close to where the boundary condition is applied), bulk waves may be observed but as the waves propagate towards the right, they dissipate all their energy into the bulk and the only remaining waves are the surface waves. Figure 5 shows the SAW amplitude as a function of depth. We see that the amplitude undergoes oscillatory (complex exponential) decay into the bulk and is negligible a few microns below the surface, again in good agreement with analytical expressions derivable from Eq. (38) [30].

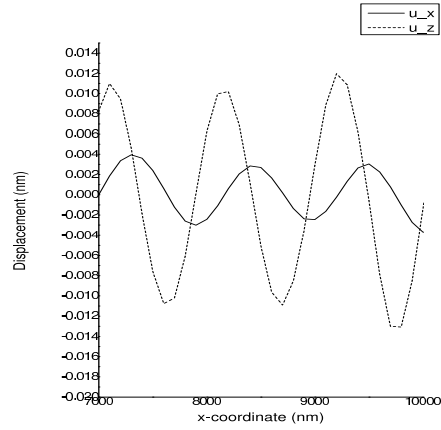


FIG. 3: The relative amplitudes and phases of the displacements u_x and u_z , parallel and perpendicular respectively, to the SAW propagation.

2. The effect of the compound mechanical structure.

Figure 6(a) shows the magnitude of the displacement field as the SAW moving from the left of the figure to the right, passes through the gate when the mechanical motion is decoupled from the electric field. The gate is centered at $(8.9 \cdot 10^3 \text{ nm}, 2.6 \cdot 10^3 \text{ nm})$. We observe a peak to the left of the gate (due to a reflection) and a trough (due to damping of the wave) to the right. We also just barely see vibrations moving away from the gate along the y direction. Since in this simulation, the mechanical motion is independent of the electric fields, this damping is due purely to the presence of a mechanical structure on the surface. The damping of the mechanical amplitude may be large enough to affect the electric potential. In this simulation, the electric potential is not affected significantly as shown in Fig. 6(b). The central blur is the electric potential due to the gate. The SAW peak

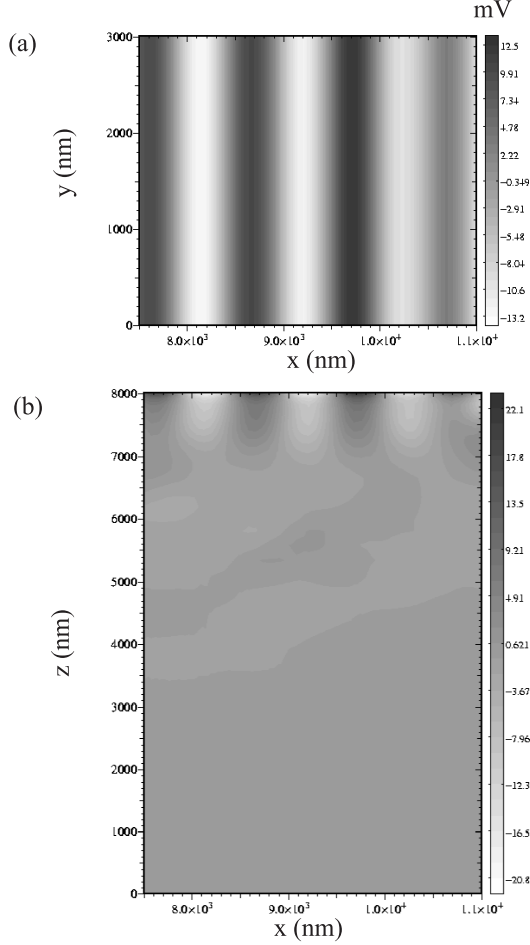


FIG. 4: (a) Plane waves of the electric potential, 100 nm below the surface, at time 1.6 ns. (b) Surface nature of the electric potential, at time 1.6 ns. The SAWs have a significant amplitude between $z = 8000$ nm and $z = 7000$ nm and have a significantly reduced amplitude below $z = 7000$ nm

emerging from the gate has been damped in the central region.

3. The effect of electromechanical coupling.

Figure 7(a) shows the magnitude of the displacement field, at time 2 ns, as the SAW passes through the gate, in the case where mutual coupling between the electric and mechanical fields is allowed. As in the decoupled case, we observe a peak to the left of the gate (due to reflection of the wave) and a trough (due to damping of the wave) to the right. Again, we also see vibrations moving away from the gate along the y direction. Comparing Figs. 6(a) and 7(a), we see that there is additional mechanical deformation throughout the material due to the presence of a charged metallic gate. Also, the scale of Fig. 7(a) is shifted up compared to that of Fig. 6(a). By

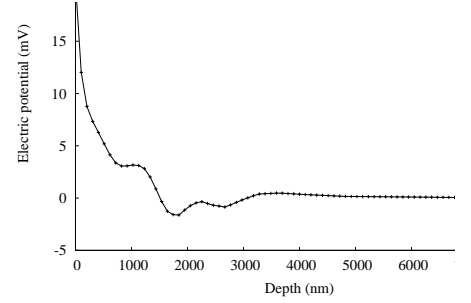


FIG. 5: A typical curve of the electric potential as a function of depth into the bulk. The precise shape of the curve clearly depends on the exact time and spatial coordinate the data was taken as the amplitude of the SAW varies from -20 mV to $+20$ mV. However, all such curves have the oscillatory decay into the bulk becoming negligible within a few microns.

looking at the displacement field at time 0 i.e. before the arrival of the SAW, we can see the displacement resulting from the applied electric field. This is shown in Fig. 7(b).

VIII. SUMMARY AND CONCLUDING REMARKS

Our aim with this paper is to suggest a computationally fast method for simulating SAWs in piezoelectric devices where stress, deformation, and a quasi-static electric field are fully coupled. The basic idea of the numerical scheme is to use a finite difference approximation in time that decouples the elasticity and the electric field problems such that these can be solved in sequence at each time level. This decoupling can also be explored in computer implementations, because independent solvers for anisotropic elasticity problems and Poisson problems can be joined together. We showed in particular how object-oriented programming techniques can realize such couplings in a very convenient way.

Through numerical experiments in a physically one-dimensional wave propagation problem we have verified that the three-dimensional code reproduces the expected quadratic convergence in space and time if linear or trilinear elements are used. Finally, we have applied the proposed numerical methodology to real SAW phenomena in a device with complicated geometry. We have described a system of boundary conditions which are capable of exciting SAW modes in a small computational domain. We have performed simulations where we have demonstrated the effects on the SAW of a charged metallic gate. The results indicate that the method is capable of predicting the expected complex elasto-electric dynamics in such a device.

The methodology could easily be applied to simulate SAWs through devices such as GaAs/AlGaAs heterostructures with more complicated surface gate geome-

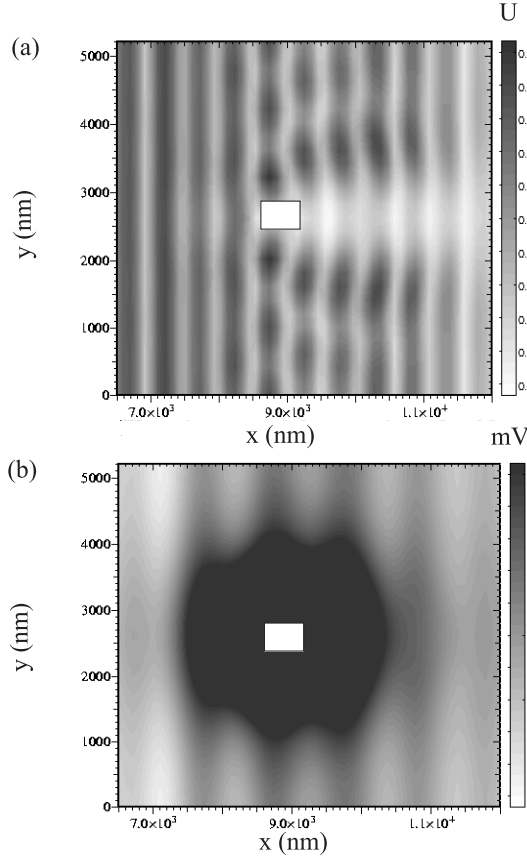


FIG. 6: (a) The magnitude of the displacement field $U = \sqrt{u_r u_r}$, at time 2 ns, as the SAW moving from left to right, passes through the gate centered at $(8.9 \cdot 10^3 \text{ nm}, 2.6 \cdot 10^3 \text{ nm})$ and shown by a white square. The mechanical motion is decoupled from the electric field. (b) The total electric potential, at time 2 ns, as the SAW passes through the gate when the mechanical motion is decoupled from the electric field. The scale has been restricted so that the SAW potential is visible. The central blur, which is due to the large external potential has the value of 1.5 V at its center. The white square shows the position of the gate.

tries.

The principal limitation of the equation splitting is a stability criterion on the time step length. Implicit methods may remove time step restrictions, but at a cost of the need to solve large coupled linear systems at each time level. The computer implementation is also more involved and requires a special-purpose solution rather than just joining two well-tested equation components. However, for wave propagation problems one usually needs a fine mesh and a small time step to resolve the waves, typically leading to $h/\Delta t = \text{const}$, which is in accordance with the stability criterion. Explicit time stepping approaches are therefore highly relevant and allow efficient algorithms and implementations.

Forthcoming numerical work will focus on domain decomposition methods for parallelizing the solver and

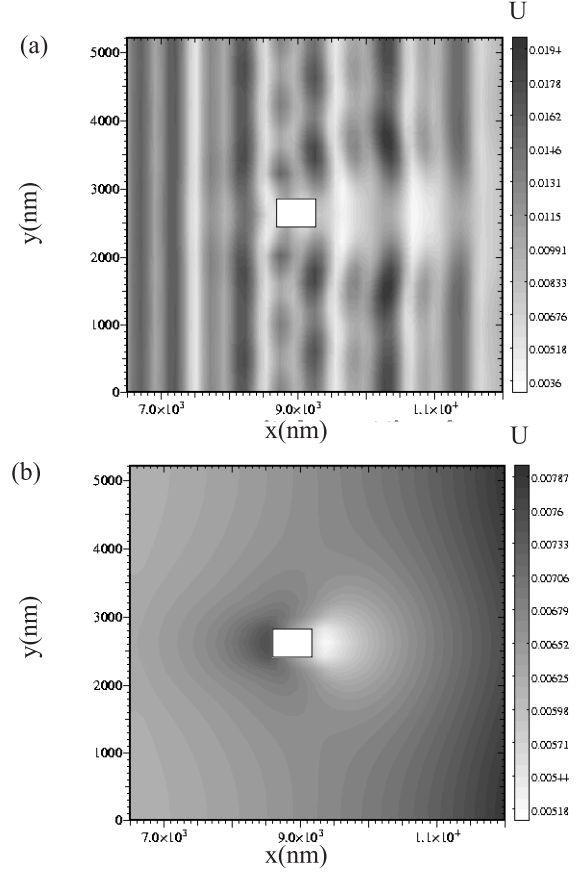


FIG. 7: (a) The magnitude of the displacement field $U = \sqrt{u_r u_r}$, at time 2 ns, as the SAW moving from left to right, passes through the gate centered at $(8.9 \cdot 10^3 \text{ nm}, 2.6 \cdot 10^3 \text{ nm})$ and shown by a white square, when full coupling between electric and mechanical fields is allowed. (b) The magnitude of the displacement field $U = \sqrt{u_r u_r}$, at time 0, demonstrating the mechanical strains caused purely by the gate with a 1.5 V applied voltage centered at $(8.9 \cdot 10^3 \text{ nm}, 2.6 \cdot 10^3 \text{ nm})$ and shown by a white square, when full coupling between electric and mechanical fields are allowed.

thereby enable simulation of large-scale SAW problems. The described time stepping approach and associated equation splitting are particularly well suited for parallel computing, because the elasticity problem can be made “perfectly parallel”, and very efficient parallelization strategies exist for the Poisson equation.

IX. ACKNOWLEDGEMENTS

We thank X. Cai and A. M. Bruaset of Simula Research Laboratory for providing assistance in the programming and debugging of the code, and M. Kataoka of the Cavendish Laboratory for useful discussions. We also acknowledge the Cambridge-MIT Institute, Darwin College Cambridge, and the Simula Research Laboratory

for financial support.

-
- [1] R. Lerch. IEEE Trans. Ultrasonics, Ferroelectrics and Frequency Control, **37**, 233, (1990).
 - [2] A. Benjeddou. Comput. Struct. A, **8**, 347, (2000).
 - [3] S. K. Ha, C. Keilers, and F. K. Chang. AIAA J., **30**, 772, (1992).
 - [4] D. A. Saravanos and P. R. Heyliger. Applied Mechanics Reviews, **52**, 305, (1999).
 - [5] S. V. Gopinathan, V. V. Varadan, and V. K. Varadan. Smart Materials and Structures, **9**, 24, (2000).
 - [6] J. Makerle. Smart materials and structures: FEM and BEM simulations - a bibliography. Finite Elements in Analysis and Design, **37**, 71, (2001).
 - [7] L. Ramdas Ram-Mohan. *Finite Element and Boundary Element Applications in Quantum Mechanics*. Oxford University Press, 1st edition, (2002).
 - [8] A. Wixforth, J. P. Kotthaus, and G. Weimann. Phys. Rev. Lett., **56**, 2104, (1986).
 - [9] J. M. Shilton, V. I. Talyanskii, M. Pepper, J. E. F. Frost, C. J. B. Ford, C. G. Smith, and G. A. C. Jones. J. Phys. Condens. Matter, **8**, 531, (1996).
 - [10] C. H. W. Barnes, J. M. Shilton, and A. M. Robinson. Phys. Rev. B, **62**, 8410, (2000).
 - [11] A. M. Robinson and C. H. W. Barnes. Phil. Trans. R. Soc. Lond., **A 361**, 1487, (2003).
 - [12] A. Bertoni, P. Bordone, R. Brunetti, C. Jacobini, and S. Reggiani. Phys. Rev. Lett., **84**, 5912, (2000).
 - [13] P. Bordone, A. Bertoni, M. Rosini, S. Reggiani, and C. Jacobini. Semicond. Sci. Tech., **19**, (2004).
 - [14] C. L. Foden, V. I. Talyanskii, G. J. Milburn, M. L. Leadbeater, and M. Pepper. Phys. Rev. A, **62**, 11803, (2000).
 - [15] J. Ebbecke, N. E. Fletcher, T. J. B. M. Janssen, F. J. Ahlers, M. Pepper, H. E. Beere and D. A. Ritchie, Phys. Lett. **84**, 4319 (2004).
 - [16] F. Alsina, P. V. Santos, H. P. Schönherr, R. Nötzel and K. H. Ploog, Phys. Rev. B **67**, 161305, (2003).
 - [17] T. Sogawa, P. V. Santos, S. K. Zhang, S. Eshlaghi, A. D. Wieck and K. H. Ploog, Phys. Rev. Lett. **87**, 276601, (2003).
 - [18] H. Matthews. Surface Wave Filters. John Wiley, 1st edition, (1977).
 - [19] J. J. Campbell and W. R. Jones. IEEE Trans. Sonics and Ultrasonics, SU15 No. **4**, 209, (1968).
 - [20] G. R. Aizin and G. Gumbs. Phys. Rev. B, **58**, 10589, (1998).
 - [21] G. Gumbs and G. R. Aizin. Phys. Rev. B, **60**, 954, (1999).
 - [22] A. Preumont. Vibration Control of Active Structures - An Introduction. Kluwer Academic Publishers, (1997).
 - [23] H. P. Langtangen. *Computational Partial Differential Equations - Numerical Methods and Diffpack Programming*. Text in Computational Science and Engineering, vol 1. Springer, 2nd edition, (2003).
 - [24] O. Zienkiewicz. The Finite Element Method. McGraw-Hill, 4th edition, (1994).
 - [25] A. Iserles, *A first course in the numerical analysis of differential equations*, Cambridge University Press, (1995).
 - [26] H. P. Langtangen. International Journal of Numerical Methods in Fluids, **10**, 213, (1989).
 - [27] R. D. Cook, D. S. Malkus, and M. E. Plesha. Concepts and Applications of Finite Element Analysis. Wiley, 3rd edition, (1989).
 - [28] H. P. Langtangen and O. Munthe. ACM Transactions on Mathematical Software, **27**, 1, March (2001).
 - [29] O. Munthe and H. P. Langtangen. Computer Methods in Applied Mechanics and Engineering, **190**, 865, (2000).
 - [30] S. H. Simon, Phys. Rev. B **54**, 13878 (1996).

A finite element method for modelling electromechanical wave propagation in anisotropic piezoelectric media

S. Rahman^{1,*}, H. P. Langtangen², and C. H. W. Barnes¹

¹*Cavendish Laboratory, Cambridge University, J J Thomson Avenue, Cambridge, CB3 0HE, United Kingdom and*

²*Simula Research Laboratory, Martin Linges v 17, Fornebu P.O.Box 134, 1325 Lysaker, Norway*

We describe and evaluate a numerical solution strategy for simulating surface acoustic waves (SAWs) through semiconductor devices with complex geometries. This multi-physics problem is of particular relevance to the design of SAW-based quantum electronic devices. The mathematical model consists of two coupled partial differential equations for the elastic wave propagation and the electric field, respectively, in anisotropic piezoelectric media. These equations are discretized by the finite element method in space and by a finite difference method in time. The latter method yields a convenient numerical decoupling of the governing equations. We describe how a computer implementation can utilize the decoupling and, via object-oriented programming techniques reuse independent codes for the Poisson equation and the linear time-dependent elasticity equation. First we apply the simulator to a simplified model problem for verifying the implementation, and thereafter we show that the methodology is capable of simulating a real-world case from nanotechnology, involving SAWs in a geometrically non-trivial device made of Gallium Arsenide.

I. INTRODUCTION

In the process of designing quantum electronic devices based on surface acoustic waves (SAWs) traversing piezoelectric media, it is necessary to determine the effect, on these waves of obstacles such as electrical gates on the surface, and also the effect of the SAW on the low-dimensional quantum mechanical systems such as quantum wires and quantum dots. In general, the gates have a non-trivial geometry, which necessitate numerical simulation tools. The finite element method is well suited to handle complex geometries and is widely used to model piezoelectric devices [1, 2, 3, 4, 5, 6]. The effect on the low-dimensional quantum mechanical systems would be analyzed through coupling the SAW simulator to both stationary and time-dependent Schrödinger equations [7]. This would require the development of a fast SAW simulator but also flexible and portable code.

SAWs are modes of propagation of energy along the free surface of a material such that there is no decay along the direction of propagation but there is exponential decay into the bulk. SAWs have been used in electrical sensor technologies for many decades and have also been a useful tool in probing quantum electronic structures, for example, quantum Hall liquids [8]. Recently, much experimental work has been done in the field of acoustic charge transport whereby a SAW across a GaAs/AlGaAs heterostructure is used to capture a single electron and then transport it along a one-dimensional quantum wire [9]. This would be useful in developing an accurate current standard, but more challenging proposals to use this in the burgeoning field of quantum information processing have been proposed [10, 11, 12, 13, 14]. SAWs have also been utilized for both static quantum dot [15] and photo-luminescence experiments [16, 17]. The time and resources required to build such devices are immense, and therefore the mathematical modelling of these devices before the physical construction is advantageous. This approach requires the solution of the continuum electromechanical equations of motion in a piezoelectric medium. The method of partial waves [18] can be used to obtain simple analytical expressions for the waves in the bulk material, but the solutions say nothing about the effect of gates on the surface. Attempts to solve the governing equations analytically for devices which do have surface gates [19, 20, 21] involve simplifications, and the accuracy of these approximations remains uncertain.

There is a vast amount of literature on the three-dimensional finite element analysis of piezoelectric devices [1, 2, 3, 4, 5, 6], and these methods are exploited in the field of ultrasonics to design control systems involving piezoelectric actuators and sensors [22]. Commercial software such as ANSYS and ABAQUS can be used to simulate electromechanical phenomena but lack the flexibility to couple to quantum mechanical calculations such as iterative Poisson-Schrödinger [7]. Therefore it is often necessary to develop one's own computer code for modelling such devices.

In this paper, we formulate and evaluate a finite element based solution method for the equations governing SAWs in piezoelectric media, and we formulate it in a flexible and portable manner to allow the ability to interface with

*Electronic address: S.Rahman.00@cantab.net

other code. The implementation is performed in an object-oriented style in order to incorporate existing solvers and to enhance portability of the code. Such a tool can be valuable in the design of micro- and nano-scale devices. We describe a set of boundary conditions that are capable of efficiently exciting SAWs and demonstrate the propagation of SAWs through a GaAs-based device. Although our applications are specific to GaAs, the formulation is general enough to allow simulations, with the same code (or with small modifications), of any crystal structure provided the elastic and piezoelectric material parameters are known.

This paper is organized as follows. In Section II we give an overview of the mathematical model underlying piezoelectricity and precisely state the coupled partial differential equations we aim to solve. Sections III and IV concern finite element formulations of these equations and an overview of the computational algorithm is described. In section V we describe the class based simulator approach used in our code design which simplifies implementation and increases reliability. Section VI presents a verification of the implementation and an empirical estimation of convergence properties of the numerical solution method. A real-world application of the methodology, concerning a SAW problem in nanotechnology is the subject of Section VII, before we make some concluding remarks in the final section.

II. MODELLING OF PIEZOELECTRIC MATERIALS

For piezoelectric materials, the electric displacement depends on both the applied electric field and mechanical strain, and the stresses depend on both the applied mechanical strain and applied electric field. The electric displacement D_i is given by

$$D_i = \epsilon_{ij}^S E_j + e_{ijk} \varepsilon_{jk}, \quad (1)$$

where E_j denotes the electric field, ϵ_{ij} is the permittivity tensor, e_{ijk} is the piezoelectric coupling constant, ε_{ij} is the strain tensor. The stress tensor σ_{ij} is given by

$$\sigma_{ij} = -e_{kij} E_k + c_{ijkl}^E \varepsilon_{kl}, \quad (2)$$

where c_{ijkl} represents the 4th rank tensor of elastic parameters. Summation over repeated indices is implied in this section, and the superscripts S and E denote that the quantities were measured under constant strain and constant electric field, respectively.

In the absence of free charges within the material, Gauss's law requires the divergence of the electric displacement to vanish:

$$\nabla \cdot D = \rho_{\text{free}} = 0. \quad (3)$$

Combining Eqs. (1) and (2), and the relation

$$E_i = -\frac{\partial \phi}{\partial x_i} \quad (4)$$

between the electric potential ϕ and the electric field E_i , together with the strain-displacement relation for small strains,

$$\varepsilon_{ij} = \frac{1}{2} \left(\frac{\partial u_j}{\partial x_i} + \frac{\partial u_i}{\partial x_j} \right), \quad (5)$$

where u_i is the mechanical displacement field, we can derive a scalar partial differential equation for ϕ :

$$\frac{\partial}{\partial x_i} \epsilon_{ik}^S \frac{\partial \phi}{\partial x_k} = \frac{\partial}{\partial x_i} e_{ikl} \frac{\partial u_l}{\partial x_k}. \quad (6)$$

This equation couples the potential ϕ and the displacements u_i in the medium, and can be used to compute the electric field. Equation (4) assumes the quasi-static approximation, which requires that very little energy is carried away by electromagnetic waves.

The displacement field in the medium is governed by Newton's 2nd law of motion combined with the appropriate constitutive law. The former equation reads

$$\rho \ddot{u}_i = \frac{\partial \sigma_{ij}}{\partial x_j} + \rho b_i, \quad (7)$$

where b_i denotes body forces, and the double dot in \ddot{u}_i denotes a second-order partial derivative in time. As Eq. (7) stands, it contains no damping term, which is irrelevant in our application setting. The constitutive law stated in Eq. (2) relates the stress tensor σ_{ij} to the strain tensor ε_{ij} , and Eq. (5) relates ε_{ij} to the displacement field u_i . Combining Eqs. (2), (5), (7), we arrive at an equation for u_i in terms of ϕ :

$$\rho \ddot{u}_i = \frac{\partial}{\partial x_j} c_{ijkl}^E \frac{\partial u_l}{\partial x_k} + \rho b_i + \frac{\partial}{\partial x_j} e_{kij} \frac{\partial \phi}{\partial x_k}. \quad (8)$$

From Eq. (8) we see how the mechanical motion is affected the electric field. In most materials, this coupling is weak, because $e_{ijk} \ll c_{ijkl}^E$, and the effect of the piezoelectric potential on the mechanical deformation is negligible. On the other hand, the effect of the mechanical deformation on the potential is always significant according to Eq. (6). However, in cases where an external electric field is applied through surface gates, the term in ϕ may be sufficiently large to contribute significantly to the mechanical motion, and these cases receive the focus of the present paper.

To illustrate the nature of these equations we explicitly write out the coupling terms for the piezoelectric material GaAs. The elastic parameters of a crystal are usually given in a coordinate system with its x , y and z axes parallel to the crystal X, Y and Z axes. For consistency with acoustoelectric charge transport experiments, we align the positive x axis with the crystal positive [011] axes, and the positive z axis with the crystal positive [100] axis. To achieve this we perform a 45 degree rotation of the crystal, around the z axis.

In the transformed frame, the only non-zero components of the piezoelectric tensor are $e_{15} = -e_{24} = e_{31} = -e_{32}$. For generality, we illustrate our method using the different values of the piezoelectric tensor. Using the assumptions stated in the previous paragraph, and neglecting body forces, we can write out equations Eqs. (8) and (6) as

$$\rho \ddot{u}_x = \frac{\partial}{\partial x_j} c_{xjkl}^E \frac{\partial u_l}{\partial x_k} + \frac{\partial}{\partial x} e_{31} \frac{\partial \phi}{\partial z} + \frac{\partial}{\partial z} e_{15} \frac{\partial \phi}{\partial x}, \quad (9)$$

$$\rho \ddot{u}_y = \frac{\partial}{\partial x_j} c_{yjkl}^E \frac{\partial u_l}{\partial x_k} + \frac{\partial}{\partial y} e_{32} \frac{\partial \phi}{\partial z} + \frac{\partial}{\partial z} e_{24} \frac{\partial \phi}{\partial y}, \quad (10)$$

$$\rho \ddot{u}_z = \frac{\partial}{\partial x_j} c_{zjkl}^E \frac{\partial u_l}{\partial x_k} + \frac{\partial}{\partial x} e_{15} \frac{\partial \phi}{\partial x} + \frac{\partial}{\partial y} e_{24} \frac{\partial \phi}{\partial y}, \quad (11)$$

$$\nabla \cdot \epsilon_s^S \nabla \phi = \frac{\partial}{\partial x} e_{15} \frac{\partial u_z}{\partial x} + \frac{\partial}{\partial y} e_{24} \frac{\partial u_z}{\partial y} + \frac{\partial}{\partial z} e_{31} \frac{\partial u_x}{\partial x} + \frac{\partial}{\partial x} e_{15} \frac{\partial u_x}{\partial z} + \frac{\partial}{\partial z} e_{32} \frac{\partial u_y}{\partial y} + \frac{\partial}{\partial y} e_{24} \frac{\partial u_y}{\partial z}. \quad (12)$$

In Refs. (20) and (21) analytical solutions of these equations were obtained, under the assumption that the ϕ term in Eqs. (9)–(11) can be ignored. This means that the mechanical motion is decoupled from the electric field, but an electric field is induced from the mechanical motion. The reliability of such substantial simplifications is limited to cases where the external potential ϕ is small. Also, the obtained solutions are for two-dimensional cases only and are therefore of minor interest when studying the effect of surface gates. Solving the fully coupled system of PDEs demands numerical techniques like the one described in the next section.

III. FINITE ELEMENT FORMULATION

We shall use the finite element method in space and the finite difference method in time. The reasons for applying the finite element method are the need for handling geometrically complicated domains and the fact that the method works very well for elasticity problems without coupling to ϕ as well as for the Poisson equation for ϕ .

We point out that the finite element formulation presented in this paper is independent of the choice of element shape, as this would be problem dependent. The elasticity part of the problem has three degrees of freedom - one for each component of the displacement vector. The electrical part has one degree of freedom for the electric potential.

A. The Poisson equation with piezoelectric coupling

Before continuing further, it is convenient to introduce a superscript ℓ to denote the time level, for example, ϕ^ℓ is ϕ at time level ℓ . The electrostatic potential ϕ^ℓ due to mechanical displacements u_i^ℓ in the piezoelectric material concerned is given by Eq. (12). The finite element formulation of such a Poisson equation is well covered in the literature [7, 23, 24, 25]. The basic idea is to approximate ϕ^ℓ by a linear combination of basis functions N_i , $\phi^\ell \approx \hat{\phi}^\ell = \sum_{j=1}^n N_j \phi_j^\ell$, insert $\hat{\phi}^\ell$ in the Poisson equation, and demand the residual to be orthogonal to the space spanned by $\{N_1, \dots, N_n\}$. The Laplace term is integrated by parts.

The only non-trivial aspect of the formulation in the present setting is the right-hand side, where the second-order derivatives of the elastic field demand integration by parts. The two first terms on the right-hand side of Eq. (12) give rise to an integral, which is straightforwardly integrated as

$$\begin{aligned} & - \int_{\Omega} N_i \left[\frac{\partial}{\partial x} e_{15} \frac{\partial u_z^\ell}{\partial x} + \frac{\partial}{\partial y} e_{24} \frac{\partial u_z^\ell}{\partial y} \right] d\Omega \\ &= \int_{\Omega} \left[e_{15} \frac{\partial N_i}{\partial x} \frac{\partial u_z^\ell}{\partial x} + e_{24} \frac{\partial N_i}{\partial y} \frac{\partial u_z^\ell}{\partial y} \right] d\Omega - \oint_{\partial\Omega} N_i \left[e_{15} \frac{\partial u_z^\ell}{\partial x} n_x + e_{24} \frac{\partial u_z^\ell}{\partial y} n_y \right] d\Gamma. \end{aligned} \quad (13)$$

The terms in Eq. (12), containing mixed derivatives, can be integrated by parts using a special form of Green's Theorem,

$$- \int_{\Omega} \phi \frac{\partial \psi}{\partial z} dx dy dz = \int_{\Omega} \frac{\partial \phi}{\partial z} \psi dx dy dz - \oint_{\Gamma} \phi \psi n_z d\Gamma. \quad (14)$$

The terms give rise to the integrals

$$\begin{aligned} & - \int_{\Omega} N_i \left[\frac{\partial}{\partial z} e_{31} \frac{\partial u_x^\ell}{\partial x} + \frac{\partial}{\partial x} e_{15} \frac{\partial u_z^\ell}{\partial z} + \frac{\partial}{\partial z} e_{32} \frac{\partial u_y^\ell}{\partial y} + \frac{\partial}{\partial y} e_{24} \frac{\partial u_z^\ell}{\partial z} \right] d\Omega \\ &= \int_{\Omega} \left[e_{31} \frac{\partial N_i}{\partial z} \frac{\partial u_x^\ell}{\partial x} + e_{15} \frac{\partial N_i}{\partial x} \frac{\partial u_z^\ell}{\partial z} + e_{32} \frac{\partial N_i}{\partial z} \frac{\partial u_y^\ell}{\partial y} + e_{24} \frac{\partial N_i}{\partial y} \frac{\partial u_z^\ell}{\partial z} \right] d\Omega \\ & - \oint_{\partial\Omega} N_i \left[e_{31} \frac{\partial u_x^\ell}{\partial x} n_z + e_{15} \frac{\partial u_z^\ell}{\partial z} n_x + e_{32} \frac{\partial u_y^\ell}{\partial y} n_z + e_{24} \frac{\partial u_z^\ell}{\partial z} n_y \right] d\Gamma. \end{aligned} \quad (15)$$

The finite element method applied to the equation for ϕ transforms the PDE problem to a linear system of equations,

$$\mathbf{P} \boldsymbol{\phi}^\ell = \mathbf{f}^\ell, \quad (16)$$

where the ‘stiffness’ matrix \mathbf{P} has its (i, j) element given by

$$P_{ij} = \int_{\Omega} \epsilon_s^S \left[\frac{\partial N_i}{\partial x} \frac{\partial N_j}{\partial x} + \frac{\partial N_i}{\partial y} \frac{\partial N_j}{\partial y} + \frac{\partial N_i}{\partial z} \frac{\partial N_j}{\partial z} \right] d\Omega. \quad (17)$$

The $\boldsymbol{\phi}^\ell$ vector in Eq. (16) contains the values of ϕ^ℓ at the nodal points. The i -th component f_i^ℓ of the right-hand side vector \mathbf{f}^ℓ can be written as

$$f_i^\ell = \oint_{\partial\Omega} \epsilon_s^S N_i \frac{\partial \phi^\ell}{\partial n} d\Gamma - \oint_{\partial\Omega} N_i r d\Gamma + \int_{\Omega} s d\Omega, \quad (18)$$

with

$$\begin{aligned} r &= e_{31} \frac{\partial u_x^\ell}{\partial x} n_z + e_{15} \frac{\partial u_x^\ell}{\partial z} n_x + e_{32} \frac{\partial u_y^\ell}{\partial y} n_z + e_{24} \frac{\partial u_y^\ell}{\partial z} n_y + e_{15} \frac{\partial u_z^\ell}{\partial x} n_x + e_{24} \frac{\partial u_z^\ell}{\partial y} n_y, \\ s &= e_{31} \frac{\partial N_i}{\partial z} \frac{\partial u_x^\ell}{\partial x} + e_{15} \frac{\partial N_i}{\partial x} \frac{\partial u_z^\ell}{\partial z} + e_{32} \frac{\partial N_i}{\partial z} \frac{\partial u_y^\ell}{\partial y} + e_{24} \frac{\partial N_i}{\partial y} \frac{\partial u_z^\ell}{\partial z} + e_{15} \frac{\partial N_i}{\partial x} \frac{\partial u_z^\ell}{\partial x} + e_{24} \frac{\partial N_i}{\partial y} \frac{\partial u_z^\ell}{\partial y}. \end{aligned}$$

When the displacement field entering f_i^ℓ is known, any standard Poisson solver can be used to compute ϕ^ℓ .

B. The elasticity problem with electric field loading

For the finite element formulation of Eq. (8) it is easier to first start with Eq. (7) and insert the constitutive law given by Eq. (2) and the strain-displacement relation given by Eq. (5) in the finite element integrals. The time derivative in Eq. (8) can be approximated by a second-order accurate finite difference. Sampling Eq. (8) at time level ℓ then yields

$$\varrho \frac{u_i^{\ell-1} - 2u_i^\ell + u_i^{\ell+1}}{\Delta t^2} = \frac{\partial \sigma_{ij}^\ell}{\partial x_j} + \varrho b_i^\ell, \quad (19)$$

where Δt is the time step length and quantities with the ℓ superscript are functions of space only. This time discretization introduces an operator splitting such that the originally coupled governing equations can be solved in sequence. No accuracy is lost by this operator splitting beyond that implied by the finite difference itself in Eq. (19). More precisely, σ_{ij}^ℓ contains ϕ^ℓ , which is known, such that we can easily solve for $u_i^{\ell+1}$ using old values of ϕ . On the next time level ($\ell + 1$), we can find $\phi^{\ell+1}$ using the recently computed $u_i^{\ell+1}$.

The main motivation for the explicit time differencing in Eq. (19) is numerical efficiency: (i) we decouple the equations, which simplifies the numerics and the implementation, and (ii) there is no need to solve large sparse linear systems of equations in the elasticity part of the problem (if the mass matrix is lumped). Nevertheless, the time difference Eq. (19) leads to a conditionally stable scheme, where Δt must be of the order of the smallest element size. In wave propagation problems, uniform high resolution is frequently needed in space and time, typically compatible with the stability restriction, which makes such explicit schemes appropriate. On the other hand, in applications where adaptive grids with great variation in element size are needed, one may benefit from implicit schemes (for example, of Newmark type) [24].

The finite element formulation of Eq. (19) is easiest to express if we switch to a typical “finite element engineering” notation, especially when we deal with anisotropic media. The stress and strain tensors are expressed as vectors,

$$\begin{aligned} \boldsymbol{\sigma} &= (\sigma_{xx}, \sigma_{yy}, \sigma_{zz}, \sigma_{yz}, \sigma_{zx}, \sigma_{yx})^T, \\ \boldsymbol{\varepsilon} &= (\varepsilon_{xx}, \varepsilon_{yy}, \varepsilon_{zz}, 2\varepsilon_{yz}, 2\varepsilon_{zx}, 2\varepsilon_{yx})^T. \end{aligned}$$

The constitutive law can then be written as

$$\boldsymbol{\sigma}^\ell = \mathbf{D} \boldsymbol{\varepsilon}^\ell + \mathbf{p}^\ell, \quad (20)$$

where the \mathbf{p}^ℓ term represents the loading from the electric field, and \mathbf{D} is a symmetric 6×6 matrix of the elasticity coefficients (previously denoted by c_{ijkl}^E):

$$\mathbf{D} = \begin{bmatrix} c_{11} & c_{12} & c_{13} & c_{14} & c_{15} & c_{16} \\ & c_{12} & c_{13} & c_{14} & c_{15} & c_{16} \\ & & c_{13} & c_{14} & c_{15} & c_{16} \\ & & & c_{14} & c_{15} & c_{16} \\ & & & & c_{15} & c_{16} \\ & & & & & c_{16} \end{bmatrix}. \quad (21)$$

The displacement field at a time level ℓ is approximated according to

$$u_i^\ell \approx \hat{\mathbf{u}}^\ell = \sum_{j=1}^n N_j \mathbf{u}_j^\ell,$$

where \mathbf{u}_j^ℓ is the value of the displacement field at node j at time level ℓ . The strain-displacement relation then becomes

$$\boldsymbol{\varepsilon}^\ell = \sum_{j=1}^n \mathbf{B}_j \mathbf{u}_j^\ell, \quad \mathbf{B}_i = \begin{bmatrix} N_{i,x} & 0 & 0 \\ 0 & N_{i,y} & 0 \\ 0 & 0 & N_{i,z} \\ 0 & N_{i,z} & N_{i,y} \\ N_{i,z} & 0 & N_{i,x} \\ N_{i,y} & N_{i,x} & 0 \end{bmatrix}. \quad (22)$$

The comma notation here denotes partial derivative: $N_{i,x} \equiv \partial N_i / \partial x$.

A finite element formulation of Eq. (19) using the aforementioned notation becomes (see Ref. 23 for a detailed derivation without the ϕ term)

$$\int_{\Omega} \varrho N_i \sum_{j=1}^n N_j (\mathbf{u}_j^{\ell-1} - 2\mathbf{u}_j^\ell + \mathbf{u}_j^{\ell+1}) d\Omega + \Delta t^2 \int_{\Omega} \mathbf{B}_i^T \boldsymbol{\sigma}^\ell d\Omega = \Delta t^2 \int_{\Omega} \varrho \mathbf{b} N_i d\Omega + \Delta t^2 \int_{\partial\Omega} \mathbf{t}^\ell N_i d\Gamma. \quad (23)$$

Here, \mathbf{t}^ℓ is the traction on the boundary, arising from integrating the divergence of the stress in Eq. (19) by parts. Inserting the constitutive law in the term $\int_{\Omega} \mathbf{B}_i^T \boldsymbol{\sigma}^\ell d\Omega$ yields

$$\sum_{j=1}^n \left(\int_{\Omega} \mathbf{B}_i^T \mathbf{D} \mathbf{B}_j d\Omega \right) \mathbf{u}_j^\ell + \int_{\Omega} \mathbf{B}_i^T \mathbf{p}^\ell d\Omega.$$

The final discrete equations arising from the equation of motion can be written as

$$\mathbf{u}^{\ell+1} = 2\mathbf{u}^\ell - \mathbf{u}^{\ell-1} + \Delta t^2 \tilde{\mathbf{M}}^{-1} (-\mathbf{K} \mathbf{u}^\ell + \boldsymbol{\beta}^\ell + \boldsymbol{\Phi}^\ell), \quad (24)$$

where $\tilde{\mathbf{M}}^{-1}$ is an efficient inverse of the mass matrix \mathbf{M} resulting from the $\int_{\Omega} \varrho N_i N_j d\Omega$ integral. We construct $\tilde{\mathbf{M}}^{-1}$ as the inverse of the lumped mass matrix (using the row-sum technique to lump the matrix). The matrix \mathbf{K} stems from the standard “stiffness” term $\int_{\Omega} \mathbf{B}_i^T \mathbf{D} \mathbf{B}_j d\Omega$ representing anisotropic elasticity, $\boldsymbol{\beta}^\ell$ is the effect of body forces and surface tractions, and $\boldsymbol{\Phi}^\ell$ is the contribution from the electric field. The i -th block (arising from node i) in $\boldsymbol{\Phi}^\ell$ takes the form $\boldsymbol{\Phi}_i^\ell = \int_{\Omega} \mathbf{B}_i^T \mathbf{p}^\ell$, which from Eqs. (9) to (11) results in

$$\boldsymbol{\Phi}_i^\ell = \begin{bmatrix} \int_{\Omega} N_i [\frac{\partial}{\partial x} e_{31} \frac{\partial \phi^\ell}{\partial z} + \frac{\partial}{\partial z} e_{15} \frac{\partial \phi^\ell}{\partial x}] d\Omega \\ - \int_{\Omega} N_i [\frac{\partial}{\partial y} e_{32} \frac{\partial \phi^\ell}{\partial z} + \frac{\partial}{\partial z} e_{24} \frac{\partial \phi^\ell}{\partial y}] d\Omega \\ \int_{\Omega} N_i [\frac{\partial}{\partial x} e_{15} \frac{\partial \phi^\ell}{\partial x} + \frac{\partial}{\partial y} e_{24} \frac{\partial \phi^\ell}{\partial y}] d\Omega \end{bmatrix}$$

$$= \begin{bmatrix} - \int_{\Omega} [e_{31} \frac{\partial N_i}{\partial x} \frac{\partial \phi^\ell}{\partial z} + e_{15} \frac{\partial N_i}{\partial z} \frac{\partial \phi^\ell}{\partial x}] d\Omega + \int_{\partial\Omega} N_i [e_{31} \frac{\partial \phi^\ell}{\partial z} n_x + e_{15} \frac{\partial \phi^\ell}{\partial x} n_z] d\Gamma \\ \int_{\Omega} [e_{32} \frac{\partial N_i}{\partial y} \frac{\partial \phi^\ell}{\partial z} + e_{24} \frac{\partial N_i}{\partial z} \frac{\partial \phi^\ell}{\partial y}] d\Omega - \int_{\partial\Omega} N_i [e_{32} \frac{\partial \phi^\ell}{\partial z} n_y + e_{24} \frac{\partial \phi^\ell}{\partial y} n_z] d\Gamma \\ - \int_{\Omega} [e_{15} \frac{\partial N_i}{\partial x} \frac{\partial \phi^\ell}{\partial x} + e_{24} \frac{\partial N_i}{\partial y} \frac{\partial \phi^\ell}{\partial y}] d\Omega + \int_{\partial\Omega} N_i [e_{15} \frac{\partial \phi^\ell}{\partial x} n_x + e_{24} \frac{\partial \phi^\ell}{\partial y} n_y] d\Gamma \end{bmatrix}. \quad (25)$$

Our governing equations require initial conditions. Let us assume that the elastic body is at rest such that $\partial u_i / \partial t = 0$. The external electric field is then turned on. After the initial transients the displacement field have faded out, and we have a stationary initial state of our system, modeled by the equations

$$\mathbf{P} \phi^0 = \mathbf{f}^0(\mathbf{u}^0), \quad (26)$$

$$\mathbf{K} \mathbf{u}^0 = \boldsymbol{\beta}^0 + \boldsymbol{\Phi}^0(\phi^0). \quad (27)$$

These two coupled equations are solved by an iterative Gauss-Seidel-like technique, i.e., the equations are solved one at a time, using the most recent approximation of the other field in the right-hand side term. Each linear system is solved by a MILU preconditioned conjugate gradient method [26]. The solution of Eqs. (26) and (27), along with the assumption of stationarity, $\partial \mathbf{u}/\partial t = 0$, comprise the initial condition.

As boundary conditions, we either have prescribed traction components or prescribed displacement components, along with prescribed electric potential or prescribed normal component of the electric field. The displacement equation needs three boundary conditions at each point at the boundary, while the equation for ϕ needs one condition at each point.

From $\partial \mathbf{u}/\partial t = 0$ at $t = 0$ it follows by a second-order difference approximation that $\mathbf{u}^1 = \mathbf{u}^{-1}$. From Eqs. (24) and (27) it follows that $\mathbf{u}^1 = \mathbf{u}^0 = \mathbf{u}^{-1}$. The loads removed at $t = 0^+$ will first come into play at the second time level.

The computational algorithm can now be formulated as follows:

```

 $\ell = 0$  (time level counter)
 $k = 0$  (iteration counter)
while  $\varepsilon < \varepsilon_{crit}$ 
    solve Eq. (26) w.r.t  $\phi^{0,k}$ 
    solve Eq. (27) w.r.t  $\mathbf{u}^{0,k}$ 
    compute  $\varepsilon = \|\mathbf{u}^{0,k} - \mathbf{u}^{0,k-1}\| + \|\phi^{0,k} - \phi^{0,k-1}\|$ 
     $k \leftarrow k + 1$  end while
 $\phi^1 = \phi^0, \mathbf{u}^1 = \mathbf{u}^0$ 
for  $\ell = 1, 2, 3, \dots$  until end of simulation
    solve Eq. (24) w.r.t  $\mathbf{u}^{\ell+1}$ 
    solve Eq. (16) w.r.t  $\phi^{\ell+1}$ 

```

Comments on Stability. The stability criterion of the explicit finite difference scheme in time, when decoupled from the electric field problem, requires $\Delta t \leq 2/\omega_{\max}$ [27], where ω_{\max} is the highest natural frequency of the vibrating system. One may find ω_{\max} as the square root of the largest eigenvalue of the problem $\mathbf{K} - \lambda \mathbf{M} = 0$. An approximate bound on ω_{\max} can be estimated from a relation $\omega_{\max} = 2c/h_{\text{eff}}$, where c is the speed of elastic waves and h_{eff} is the smallest effective element length. The stability criterion now reduces to the common Courant, Friedrichs, and Lewy (CFL) condition:

$$\Delta t \leq \alpha h_{\text{eff}}/c. \quad (28)$$

Here, α is a factor to be adjusted since the h_{eff} parameter is normally roughly computed from element sizes or application of Gerschgorin's theorem applied to the underlying eigenvalue problem. For wave problems the CFL condition is frequently not particularly restrictive since the length and period of a wave are usually proportional, leading to a natural choice of $\Delta t/h = \text{const.}$

IV. AN OPTIMISED FINITE ELEMENT FORMULATION

We can speed up the numerical computation by replacing the complete assembly of the right-hand side vectors in Eqs. (16) and (24) by a matrix-vector product. For example, consider the contribution to the vector \mathbf{f} in Eq. (16) due to the coupling from the mechanical motion (omitting the superscript ℓ for the remainder of this section):

$$\int_{\Omega} e_{31} \frac{\partial N_i}{\partial z} \frac{\partial u_x}{\partial x} + e_{15} \frac{\partial N_i}{\partial x} \frac{\partial u_x}{\partial z} + e_{32} \frac{\partial N_i}{\partial z} \frac{\partial u_y}{\partial y} + e_{24} \frac{\partial N_i}{\partial y} \frac{\partial u_y}{\partial z} + e_{15} \frac{\partial N_i}{\partial x} \frac{\partial u_z}{\partial x} + e_{24} \frac{\partial N_i}{\partial y} \frac{\partial u_z}{\partial y} d\Omega. \quad (29)$$

Inserting the finite element expansion $u_x \approx \sum_{j=1}^n u_j^{(x)} N_j$, and similar expansions for u_y and u_z , the expression in Eq. (29) results in

$$\begin{aligned} & \sum_{j=1}^n \int_{\Omega} e_{31} \frac{\partial N_i}{\partial z} \frac{\partial N_j}{\partial x} u_j^{(x)} + e_{15} \frac{\partial N_i}{\partial x} \frac{\partial N_j}{\partial z} u_j^{(x)} + e_{32} \frac{\partial N_i}{\partial z} \frac{\partial N_j}{\partial y} u_j^{(y)} \\ & + e_{24} \frac{\partial N_i}{\partial y} \frac{\partial N_j}{\partial z} u_j^{(y)} + e_{15} \frac{\partial N_i}{\partial x} \frac{\partial N_j}{\partial x} u_j^{(z)} + e_{24} \frac{\partial N_i}{\partial y} \frac{\partial N_j}{\partial y} u_j^{(z)} d\Omega. \end{aligned} \quad (30)$$

This expression can be written as a matrix vector product $\mathbf{L}\mathbf{u}$, where the matrix \mathbf{L} consists of $n \times n$ blocks, each block of size 1×3 . For the coupling of node i and j , the 3×1 block looks like

$$e_{31} \frac{\partial N_i}{\partial z} \frac{\partial N_j}{\partial x} + e_{15} \frac{\partial N_i}{\partial x} \frac{\partial N_j}{\partial z}, e_{32} \frac{\partial N_i}{\partial z} \frac{\partial N_j}{\partial y} + e_{24} \frac{\partial N_i}{\partial y} \frac{\partial N_j}{\partial z}, e_{15} \frac{\partial N_i}{\partial x} \frac{\partial N_j}{\partial x} + e_{24} \frac{\partial N_i}{\partial y} \frac{\partial N_j}{\partial y}, \quad (31)$$

The Poisson equation - Eq. (16) for ϕ can now be written as

$$\mathbf{P}\phi^{\ell+1} = \mathbf{L}\mathbf{u}^{\ell+1}. \quad (32)$$

At each time level we can hence avoid the costly finite element assembly process, since \mathbf{P} and \mathbf{L} are constant in time and the right-hand side of the linear system is obtained by an efficient matrix-vector product. This may result in a significant speed-up of the solver. For large number of unknowns, the speed up is experienced only if we use a method of complexity or order n , like multigrid, to solve Eq. (32).

Equation (24) is already on a favorable matrix-vector algebra form, except for the coupling term Φ^ℓ . Examining Eq. (25), we realize that this matrix can be written as $\Phi^\ell = \mathbf{Q}\phi^\ell$, where \mathbf{Q} is a time-independent $n \times n$ matrix of 3×1 blocks. The contribution to block i in Φ^ℓ is made of the coupling \mathbf{Q}_{ij} between node i and j and the block j in ϕ^ℓ : $\Phi_i^\ell = \mathbf{Q}_{ij}\phi_j^\ell$, where

$$\mathbf{Q}_{ij} = \begin{bmatrix} -\int_{\Omega} e_{31} \frac{\partial N_i}{\partial x} \frac{\partial N_j}{\partial z} + e_{15} \frac{\partial N_i}{\partial z} \frac{\partial N_j}{\partial x} d\Omega + \int_{\partial\Omega} N_i [e_{31} \frac{\partial N_j}{\partial z} n_x + e_{15} \frac{\partial N_j}{\partial x} n_z] d\Gamma \\ \int_{\Omega} e_{32} \frac{\partial N_i}{\partial y} \frac{\partial N_j}{\partial z} + e_{24} \frac{\partial N_i}{\partial z} \frac{\partial N_j}{\partial y} d\Omega - \int_{\partial\Omega} N_i [e_{32} \frac{\partial N_j}{\partial z} n_y + e_{24} \frac{\partial N_j}{\partial y} n_z] d\Gamma \\ -\int_{\Omega} e_{15} \frac{\partial N_i}{\partial x} \frac{\partial N_j}{\partial x} + e_{24} \frac{\partial N_i}{\partial y} \frac{\partial N_j}{\partial y} d\Omega + \int_{\partial\Omega} N_i [e_{15} \frac{\partial N_j}{\partial x} n_x + e_{24} \frac{\partial N_j}{\partial y} n_y] d\Gamma \end{bmatrix}.$$

Now the Φ^ℓ term in Eq. (24) can be computed as a matrix-vector product $\mathbf{Q}\phi^\ell$, and no assembly process is required to construct Eq. (24) at each time level. In our algorithm we must run assembly processes at $t = 0$ to construct the matrices $\tilde{\mathbf{M}}^{-1}$, \mathbf{K} , \mathbf{Q} , \mathbf{L} , and \mathbf{P} .

V. OBJECT-ORIENTED IMPLEMENTATION

A significant trend in modern software development is to formulate numerical algorithms such that reliable and well-tested software components can be combined together to form a new simulator. Our numerical approach was in particular inspired by such an approach. With the time discretization we were able to split the coupled u_i - ϕ system such that at each time level we first solve for a new displacement field (u_i) and then we solve for the corresponding electric potential (ϕ). In each of the two equations, the effect of the other only enters through a right-hand side “forcing” term. This allows us, in principle, to reuse a solver for elastic vibrations and a Poisson solver, as long as these solvers can implement a new right-hand side term that couples to another solver. From a principal point of view, this idea is simple and attractive. However, the implementation of the idea in practice may be less feasible if the design of the underlying solvers is not sufficiently flexible.

To allow for building the compound u_i - ϕ solver from separate u_i and ϕ solvers we propose to apply principles from object-oriented programming. The time-dependent elasticity solver and the Poisson solver are realized as two independent objects, implemented via classes in C++. Actually, we have reused the `Poisson2` class from Ref. 23 as the Poisson solver, and the `ElasticVib1` class from Ref. 23 as the elastic vibration solver. The latter is a subclass of `Elasticity2`, a pure quasi time-dependent elasticity solver (without the acceleration term in the momentum equation). These classes are implemented using building blocks from the Diffpack library [23].

The `Poisson2` and `ElasticVib1` classes have no knowledge of each other. The only common feature is their design. This design is crucial for reuse of the classes to solve the coupled problem, but the design approach suggested for Diffpack solvers [23, 28, 29] has proven to be successful in this respect. Diffpack solvers are realized as classes containing objects for grids, scalar/vector fields, linear systems, etc. The coefficients in a PDE are evaluated through virtual functions. When the solver is stand-alone, these virtual functions contain mathematical expressions or measured data, but when solvers are combined, the virtual functions are reimplemented in subclasses and connected to data in other solvers. This principle reflects the underlying mathematics: the coefficients in a single PDE are considered known, but in a system of PDEs, the coefficients typically couple to unknown quantities governed by the PDEs. The present coupled system is an example where the right-hand side in the Poisson equation couples to the primary unknown

in the elastic vibration solver, while a right-hand side term in the elastic vibration solver couples to the primary unknown in the Poisson equation. When the solvers are used independently there are no such couplings.

Figure 1 shows an outline of the class design for the compound solver. From class `Poisson2` we derive a subclass `Poisson2_glue`, which reimplements the virtual function in `Poisson2` for evaluating the right-hand side in that equation. In this new function we need to compute an expression involving the displacement field available in the `ElasticVib1` class. A manager class, simply called `Manager`, holds pointers to all classes for the individual PDEs in the system of PDEs, and each PDE class holds a pointer to the manager class, thus enabling a two-way communication. With these pointers, we can connect data from any other solver class to the `Poisson2_glue` class. In the virtual function evaluating the right-hand side we can typically call `mng->elastic->u` to get a vector field object for u_i that we can evaluate at the current integration point. This object has support for evaluating derivatives of the field as well.

Similarly, we derive a subclass `ElasticVib1_glue` of `ElasticVib1`, add a pointer to the manager class, and override the virtual function for evaluating the right-hand side. Now we need to compute expressions involving ϕ , but this is easily accomplished by the pointers, e.g., `mng->poisson->u` if u is the name of the unknown scalar field in the `Poisson2` solver.

The “glue” classes `Poisson2_glue` and `ElasticVib1_glue` are very small compared to the real solver classes they inherit from. A “glue” class typically needs about a page of code unless it adds additional computations. The manager class is a bit more comprehensive since it implements the overall solution algorithm, i.e., the time stepping and the calls to the independent solvers.

The benefit from using object-oriented programming in the way we have outlined is that the original well-tested Poisson and elastic vibration solvers can be reused in a system of PDEs without any modifications. The original solver classes reside in separate files and are hence not subject to any side effects from editing the source code. The “glue” class is also in a separate file and enables the original solver to speak to a manager in charge of solving a compound system of PDEs. The advantages are clear: reliability is increased by reusing well-tested solvers, and the compound solver is modularized. Our experience is that this design reduces the development time significantly. Especially the debugging phase is greatly simplified. At any time, the underlying solvers can be trivially pulled out of the compound system and verified independently.

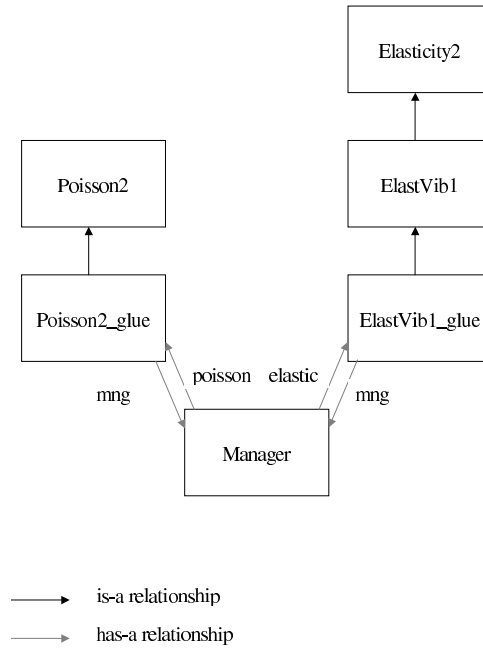


FIG. 1: Relationships between classes. The base classes, `Poisson2` and `Elasticity2` perform the solution of the standard time-independent Poisson and elasticity equations, respectively. `ElasticVib1` is derived from `Elasticity2` and solves for time-dependent elastic motion. The classes `Poisson2_glue` and `ElasticVib1_glue` implement the coupling between the electrostatic and mechanical equations, and these classes are controlled by the `Manager` class.

VI. VERIFICATION

Before showing numerical results for a physically relevant application, we report on the estimated numerical accuracy of the code, thereby establishing evidence for the correctness of the implementation. To investigate numerical errors, we compare numerical results with an exact solution. The exact solution is based on the assumption of a displacement field in z direction only, depending on x and t only. Physically, a normal traction is applied at all $x = \text{const}$ and $y = \text{const}$ boundaries to avoid displacements in the x and y directions, but in the code we implement this situation by essential boundary conditions $u_x = u_y = 0$. We also assume that $\phi = \phi(x, t)$ and that the material is isotropic. The governing equations then reduce to

$$\rho \ddot{u}_z = \mu \frac{\partial^2 u_z}{\partial x^2} + e_{15} \frac{\partial^2 \phi}{\partial x^2}, \quad (33)$$

$$\epsilon_s \frac{\partial^2 \phi}{\partial x^2} = e_{15} \frac{\partial^2 u_z}{\partial x^2}. \quad (34)$$

These equations can be scaled to yield

$$\ddot{u}_z = \frac{\partial^2 u_z}{\partial x^2} + \alpha \frac{\partial^2 \phi}{\partial x^2}, \quad (35)$$

$$\frac{\partial^2 \phi}{\partial x^2} = \frac{\partial^2 u_z}{\partial x^2}. \quad (36)$$

The constant α is zero or unity corresponding to whether the elasticity problem couples to the electric field problem or not. (The three coefficients in the original system are scaled away by choosing an appropriate time scale, ϕ scale, and u_i scale.) One possible solution of Eqs. (35)–(36) reads

$$u_z(x, t) = \phi(x, t) = \cos(k\sqrt{1 + \alpha}t) \sin(kx). \quad (37)$$

In our tests we choose Ω as a three-dimensional beam and $k = \frac{n\pi}{L}$, with n being an integer and L the length of the beam. The ends of the beam are then fixed.

Our verification procedure consists of estimating the convergence rate of the numerical method. A scalar error measure e is expected to behave like

$$e = Ah^r + B\Delta t^s,$$

where A and B are constants independent of the element size h and the time step Δt . From the involved approximations, we expect $s = 2$ and $r = 1 + q$, where q is the order of the polynomials in an element. In particular, for linear or trilinear elements, $r = 2$, and if h and Δt are chosen such that $h/\Delta t = \text{const}$, we see that $e \sim h^r$. From two successive experiments, (h_{i-1}, e_{i-1}) and (h_i, e_i) we may estimate a convergence rate r_i from

$$r_i = \frac{\ln e_i / e_{i-1}}{\ln h_i / h_{i-1}}.$$

We have investigated three error measures, given as different norms of the error field $E = u_z - \hat{u}_z$, where \hat{u}_z is the numerical solution and u_z is the exact solution:

$$\|E\|_{L^1(\Omega)} = \int_{\Omega} |E| d\Omega, \quad \|E\|_{L^2(\Omega)} = \left(\int_{\Omega} E^2 d\Omega \right)^{\frac{1}{2}}, \quad \|E\|_{L^\infty(\Omega)} = \sup(|E(\mathbf{x})|, \mathbf{x} \in \Omega).$$

Table I displays the values of the error norms and the associated estimates of the convergence rates r_i . As the grid spacing h and the time step Δt are reduced, the numerical solution converges to the exact solution with the expected rate of two. This provides evidence for the correctness of the implementation and indicates that our overall solution method, including the operator splitting, is of second order in time and space. The spatial convergence rate is expected to increase with the order of the polynomials used in the elements.

VII. A SURFACE ACOUSTIC WAVE APPLICATION

In order to show that our suggested numerical model may be applied to real-world phenomena, we apply it to a problem in quantum electronics, specifically in acoustic charge transport. We simulate a SAW propagating through

h	$\ E\ _{L^1}$	rates	$\ E\ _{L^2}$	rates	$\ E\ _{L^\infty}$	rates
0.05	$2.440 \cdot 10^{-5}$		$2.710 \cdot 10^{-6}$		$3.830 \cdot 10^{-7}$	
0.1	$9.760 \cdot 10^{-5}$	1.999	$1.084 \cdot 10^{-6}$	2.000	$1.533 \cdot 10^{-6}$	2.000
0.2	$3.902 \cdot 10^{-4}$	1.999	$4.335 \cdot 10^{-5}$	1.999	$6.130 \cdot 10^{-6}$	1.999
0.25	$6.096 \cdot 10^{-4}$	1.999	$6.771 \cdot 10^{-5}$	1.999	$9.574 \cdot 10^{-6}$	1.999
0.5	$2.432 \cdot 10^{-3}$	1.996	$2.702 \cdot 10^{-4}$	1.996	$3.819 \cdot 10^{-5}$	1.996

TABLE I: Error norms and estimated convergence rates for waves in a piezoelectric material, with $h = 10\Delta t$.

a nano-scale substrate of GaAs. SAWs are particular solutions of Eqs. (9) - (12) such that they propagate without decay on the surface of a material but decay exponentially into the bulk. The solutions typically have the form,

$$\begin{aligned} u_i &= \sum_j U_{i,j} e^{-kq_j z} e^{i(kx - \omega t)}, \\ \phi &= \sum_j \Phi_j e^{-kq_j z} e^{i(kx - \omega t)}, \end{aligned} \quad (38)$$

assuming x is the direction of propagation, z is the direction into the bulk ($z \rightarrow -\infty$), and the decay constants q_j , may be complex, allowing for oscillatory decay (in an exponential envelope) into the bulk as is the case for GaAs [30]. The $U_{i,j}$ and Φ_j are constant amplitudes, and k is a wavenumber. It is a straightforward mathematical procedure to determine the decay constants and wave velocity [18]. However, we are interested in the more complicated dynamics taking place when an obstacle in the form of a charged metallic gate is placed on the surface.

In acoustic charge transport, the time-varying electric potential accompanying the SAW is used to transport electrons which are trapped in the minima of the waves. To perform further manipulation on these electrons, for example, to remove some from a minimum, external electric fields must be applied, and this is achieved by applying voltages to metallic gates placed on the surface. In general, the gates have different electrical and mechanical properties to the bulk piezoelectric material and so we may expect to see interesting effects if for example a SAW is passed through the compound structure. Here, we perform three simulations where we pass a SAW through a piece of GaAs. The first will be a bare SAW, as a check to see we do excite the required modes. The following two will have a metallic gate of contrasting mechanical properties to GaAs with a static voltage applied on it. In the first of these, we decouple the mechanical motion from the electric field (while keeping the electric field coupled to the mechanical motion). In the second we allow the full mutual coupling between the electrical and mechanical fields to take place. The dimensions of the gate are $600 \text{ nm} \times 400 \text{ nm} \times 200 \text{ nm}$. To magnify the effect of the compound material structure we use a fictitious material for the gate, similar in crystal structure to GaAs, but with the elastic constants and mass density changed by one order of magnitude. Moreover, we apply a relatively large voltage of 1.5 V so that the coupling of the mechanical displacement to the electric field is evident.

In the numerical simulations we have implemented 8-noded hexahedral brick elements with $2 \times 2 \times 2$ Gauss-Legendre integration. The spacing along the direction of the SAW propagation - Δx is chosen to be 100 nm. The time integration parameter Δt is 1.25×10^{-2} ns.

A. Experiments with surface acoustic waves

In realistic SAW-based devices, bulk waves and SAWs are excited by the application of a microwave signal to an interdigitated transducer. The waves propagate outward from the source, with bulk waves dissipating energy into the bulk and surface acoustic waves travelling through the free surface. In acoustoelectric charge transport experiments, the quantum devices are located several thousand microns away from the source where one would expect to see only surface acoustic waves. To simulate the entire system would therefore require vast computational resources (the wavelength of a SAW is one micron and approximately ten nodes would be required across one wavelength for a satisfactory description). Instead we describe a system of boundary conditions which excite acoustic waves with SAWs dominating over the bulk waves within a few microns of the source.

1. Excitation of SAWs.

We point out that to be consistent with the formulation presented in the previous sections and hence acoustoelectric charge transport experiments, in our simulations the SAW travels along the crystal positive [011] axis, with the positive z axis aligned with the crystal positive [100] axis.

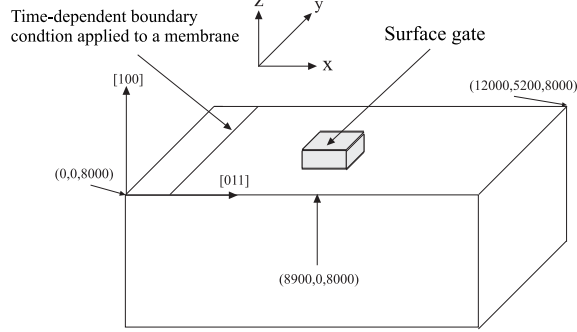


FIG. 2: A schematic diagram of the experimental setup for simulating SAWs. The gate is centered at $(8.9 \cdot 10^3 \text{ nm}, 2.6 \cdot 10^3 \text{ nm})$

In order to excite the SAW modes, we apply a time-dependent Dirichlet boundary condition to the z component of the displacement field on a small region on the grid. This can be expressed as

$$\begin{aligned} u_x = u_y = 0, \quad u_z = A \sin(2\pi ft), \\ x_0 \leq x \leq x_1, \quad z = 8000 \text{ nm}. \end{aligned} \quad (39)$$

The thickness of the membrane is defined as $x_1 - x_0 = 100 \text{ nm}$. To reduce diffraction effects from the surfaces $y = 0 \text{ nm}$ and $y = 5200 \text{ nm}$ we have forced $u_y = 0$ on those faces. The frequency f used is 2.7 GHz and the amplitude A is chosen so that the SAW amplitude is approximately 20 mV at a depth of 100 nm . Traction free boundary conditions for the mechanical equations and zero normal electrical displacements are implemented at the surfaces. We found this system of boundary conditions to be a particularly efficient means of generating coherent SAWs. The setup is shown in Fig. 2.

Figure 3 is a result of a simulation showing the $\frac{\pi}{2}$ phase difference between the x and z components of the displacement vector, and the larger z amplitude, suggesting elliptical polarization in the sagittal plane. Figures 4(a) and 4(b) show two-dimensional slices, in perpendicular planes, of the full three-dimensional solutions. The first shows the non-decaying nature of these waves along the propagation direction. The SAW wavelength can be seen to be approximately 1000 nm and its velocity is computed to be approximately $2700 \pm 20 \text{ ms}^{-1}$, which is in good agreement with analytical calculations for the wave velocity. The second figure shows the surface nature of these waves; the greatest amplitude is near the surface and there is no observable decay in the direction of propagation but they decay exponentially into the bulk. On the far left of each image (close to where the boundary condition is applied), bulk waves may be observed but as the waves propagate towards the right, they dissipate all their energy into the bulk and the only remaining waves are the surface waves. Figure 5 shows the SAW amplitude as a function of depth. We see that the amplitude undergoes oscillatory (complex exponential) decay into the bulk and is negligible a few microns below the surface, again in good agreement with analytical expressions derivable from Eq. (38) [30].

2. The effect of the compound mechanical structure.

Figure 6(a) shows the magnitude of the displacement field as the SAW moving from the left of the figure to the right, passes through the gate when the mechanical motion is decoupled from the electric field. The gate is centered at $(8.9 \cdot 10^3 \text{ nm}, 2.6 \cdot 10^3 \text{ nm})$. We observe a peak to the left of the gate (due to a reflection) and a trough (due to damping of the wave) to the right. We also just barely see vibrations moving away from the gate along the y direction. Since in this simulation, the mechanical motion is independent of the electric fields, this damping is due purely to the presence of a mechanical structure on the surface. The damping of the mechanical amplitude may be large enough to affect the electric potential. In this simulation, the electric potential is not affected significantly as shown in Fig. 6(b). The central blur is the electric potential due to the gate. The SAW peak emerging from the gate has been damped in the central region.

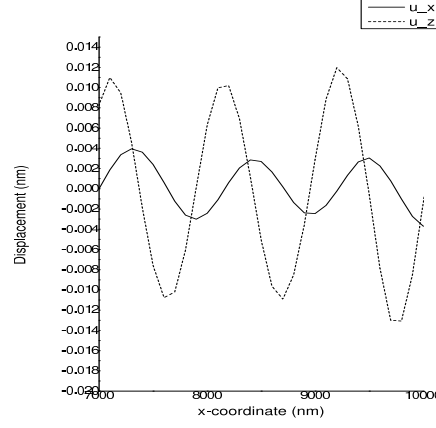


FIG. 3: The relative amplitudes and phases of the displacements u_x and u_z , parallel and perpendicular respectively, to the SAW propagation.

3. The effect of electromechanical coupling.

Figure 7(a) shows the magnitude of the displacement field, at time 2 ns, as the SAW passes through the gate, in the case where mutual coupling between the electric and mechanical fields is allowed. As in the decoupled case, we observe a peak to the left of the gate (due to reflection of the wave) and a trough (due to damping of the wave) to the right. Again, we also see vibrations moving away from the gate along the y direction. Comparing Figs. 6(a) and 7(a), we see that there is additional mechanical deformation throughout the material due to the presence of a charged metallic gate. Also, the scale of Fig. 7(a) is shifted up compared to that of Fig. 6(a). By looking at the displacement field at time 0 i.e. before the arrival of the SAW, we can see the displacement resulting from the applied electric field. This is shown in Fig. 7(b).

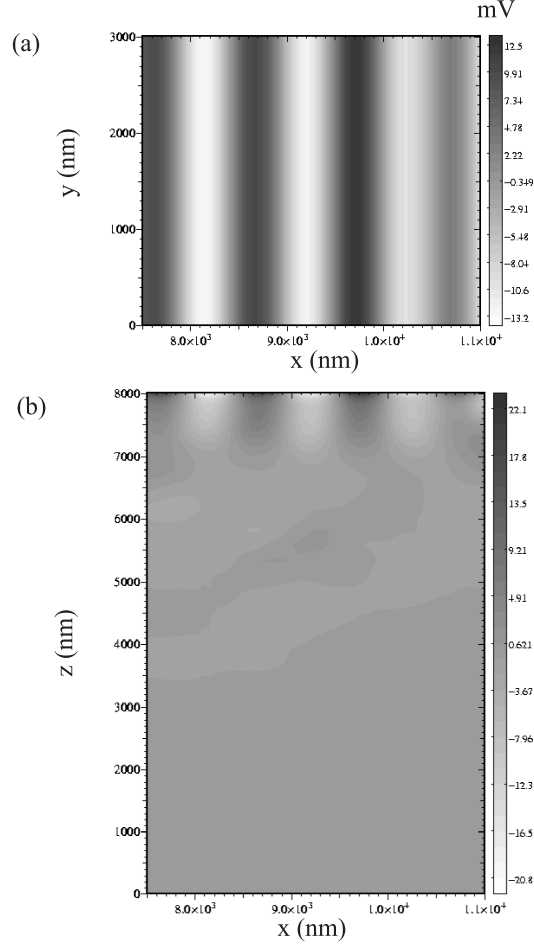


FIG. 4: (a) Plane waves of the electric potential, 100 nm below the surface, at time 1.6 ns. (b) Surface nature of the electric potential, at time 1.6 ns. The SAWs have a significant amplitude between $z = 8000$ nm and $z = 7000$ nm and have a significantly reduced amplitude below $z = 7000$ nm

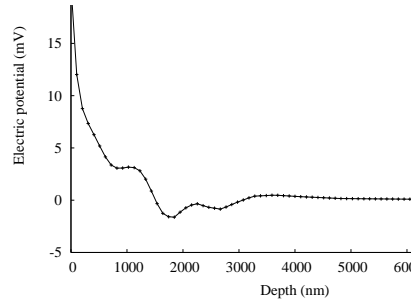


FIG. 5: A typical curve of the electric potential as a function of depth into the bulk. The precise shape of the curve clearly depends on the exact time and spatial coordinate the data was taken as the amplitude of the SAW varies from -20 mV to $+20$ mV. However, all such curves have the oscillatory decay into the bulk becoming negligible within a few microns.

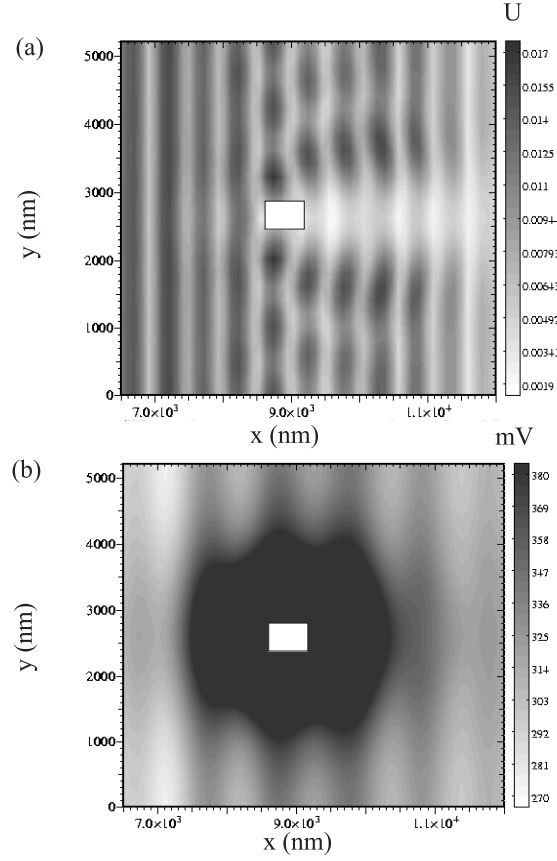


FIG. 6: (a) The magnitude of the displacement field $U = \sqrt{u_r u_r}$, at time 2 ns, as the SAW moving from left to right, passes through the gate centered at $(8.9 \cdot 10^3 \text{ nm}, 2.6 \cdot 10^3 \text{ nm})$ and shown by a white square. The mechanical motion is decoupled from the electric field. (b) The total electric potential, at time 2 ns, as the SAW passes through the gate when the mechanical motion is decoupled from the electric field. The scale has been restricted so that the SAW potential is visible. The central blur, which is due to the large external potential has the value of 1.5 V at its center. The white square shows the position of the gate.

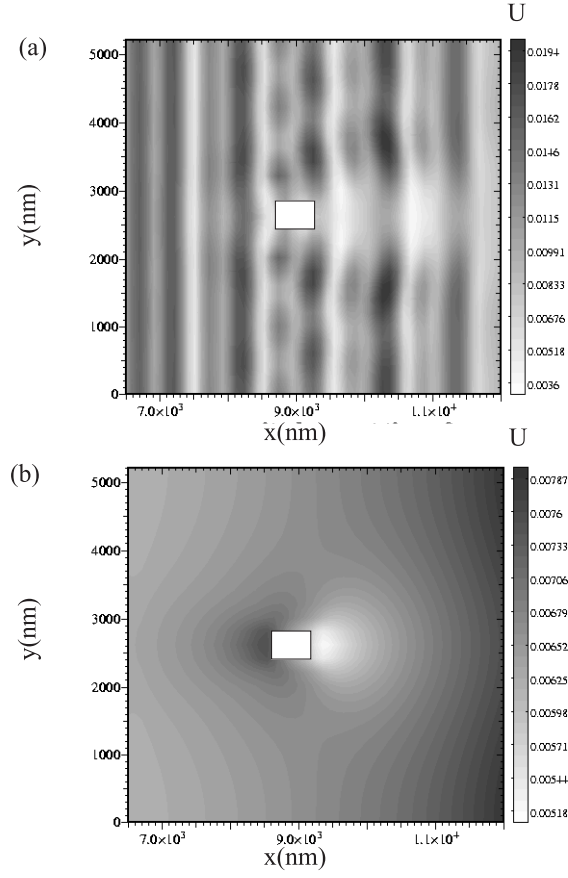


FIG. 7: (a) The magnitude of the displacement field $U = \sqrt{u_r u_r}$, at time 2 ns, as the SAW moving from left to right, passes through the gate centered at $(8.9 \cdot 10^3 \text{ nm}, 2.6 \cdot 10^3 \text{ nm})$ and shown by a white square, when full coupling between electric and mechanical fields is allowed. (b) The magnitude of the displacement field $U = \sqrt{u_r u_r}$, at time 0, demonstrating the mechanical strains caused purely by the gate with a 1.5 V applied voltage centered at $(8.9 \cdot 10^3 \text{ nm}, 2.6 \cdot 10^3 \text{ nm})$ and shown by a white square, when full coupling between electric and mechanical fields are allowed.

VIII. SUMMARY AND CONCLUDING REMARKS

Our aim with this paper is to suggest a computationally fast method for simulating SAWs in piezoelectric devices where stress, deformation, and a quasi-static electric field are fully coupled. The basic idea of the numerical scheme is to use a finite difference approximation in time that decouples the elasticity and the electric field problems such that these can be solved in sequence at each time level. This decoupling can also be explored in computer implementations, because independent solvers for anisotropic elasticity problems and Poisson problems can be joined together. We showed in particular how object-oriented programming techniques can realize such couplings in a very convenient way.

Through numerical experiments in a physically one-dimensional wave propagation problem we have verified that the three-dimensional code reproduces the expected quadratic convergence in space and time if linear or trilinear elements are used. Finally, we have applied the proposed numerical methodology to real SAW phenomena in a device with complicated geometry. We have described a system of boundary conditions which are capable of exciting SAW modes in a small computational domain. We have performed simulations where we have demonstrated the effects on the SAW of a charged metallic gate. The results indicate that the method is capable of predicting the expected complex elasto-electric dynamics in such a device.

The methodology could easily be applied to simulate SAWs through devices such as GaAs/AlGaAs heterostructures with more complicated surface gate geometries.

The principal limitation of the equation splitting is a stability criterion on the time step length. Implicit methods may remove time step restrictions, but at a cost of the need to solve large coupled linear systems at each time level. The computer implementation is also more involved and requires a special-purpose solution rather than just joining two well-tested equation components. However, for wave propagation problems one usually needs a fine mesh and a small time step to resolve the waves, typically leading to $h/\Delta t = \text{const}$, which is in accordance with the stability criterion. Explicit time stepping approaches are therefore highly relevant and allow efficient algorithms and implementations.

Forthcoming numerical work will focus on domain decomposition methods for parallelizing the solver and thereby enable simulation of large-scale SAW problems. The described time stepping approach and associated equation splitting are particularly well suited for parallel computing, because the elasticity problem can be made “perfectly parallel”, and very efficient parallelization strategies exist for the Poisson equation.

IX. ACKNOWLEDGEMENTS

We thank X. Cai and A. M. Bruaset of Simula Research Laboratory for providing assistance in the programming and debugging of the code, and M. Kataoka of the Cavendish Laboratory for useful discussions. We also acknowledge the Cambridge-MIT Institute, Darwin College Cambridge, and the Simula Research Laboratory for financial support.

-
- [1] R. Lerch. IEEE Trans. Ultrasonics, Ferroelectrics and Frequency Control, **37**, 233, (1990).
 - [2] A. Benjeddou. Comput. Struct. A, **8**, 347, (2000).
 - [3] S. K. Ha, C. Keilers, and F. K. Chang. AIAA J., **30**, 772, (1992).
 - [4] D. A. Saravanan and P. R. Heyliger. Applied Mechanics Reviews, **52**, 305, (1999).
 - [5] S. V. Gopinathan, V. V. Varadan, and V. K. Varadan. Smart Materials and Structures, **9**, 24, (2000).
 - [6] J. Makerle. Smart materials and structures: FEM and BEM simulations - a bibliography. Finite Elements in Analysis and Design, **37**, 71, (2001).
 - [7] L. Ramdas Ram-Mohan. *Finite Element and Boundary Element Applications in Quantum Mechanics*. Oxford University Press, 1st edition, (2002).
 - [8] A. Wixforth, J. P. Kotthaus, and G. Weimann. Phys. Rev. Lett., **56**, 2104, (1986).
 - [9] J. M. Shilton, V. I. Talyanskii, M. Pepper, J. E. F. Frost, C. J. B. Ford, C. G. Smith, and G. A. C. Jones. J. Phys. Condens. Matter, **8**, 531, (1996).
 - [10] C. H. W. Barnes, J. M. Shilton, and A. M. Robinson. Phys. Rev. B, **62**, 8410, (2000).
 - [11] A. M. Robinson and C. H. W. Barnes. Phil. Trans. R. Soc. Lond., **A 361**, 1487, (2003).
 - [12] A. Bertoni, P. Bordone, R. Brunetti, C. Jacobini, and S. Reggiani. Phys. Rev. Lett., **84**, 5912, (2000).
 - [13] P. Bordone, A. Bertoni, M. Rosini, S. Reggiani, and C. Jacobini. Semicond. Sci. Tech., **19**, (2004).
 - [14] C. L. Foden, V. I. Talyanskii, G. J. Milburn, M. L. Leadbeater, and M. Pepper. Phys. Rev. A, **62**, 11803, (2000).
 - [15] J. Ebbecke, N. E. Fletcher, T. J. B. M. Janssen, F. J. Ahlers, M. Pepper, H. E. Beere and D. A. Ritchie, Phys. Lett. **84**, 4319 (2004).
 - [16] F. Alsina, P. V. Santos, H. P. Schönherr, R. Nötzel and K. H. Ploog, Phys. Rev. B **67**, 161305, (2003).
 - [17] T. Sogawa, P. V. Santos, S. K. Zhang, S. Eshlaghi, A. D. Wieck and K. H. Ploog, Phys. Rev. Lett. **87**, 276601, (2003).

- [18] H. Matthews. Surface Wave Filters. John Wiley, 1st edition, (1977).
- [19] J. J. Campbell and W. R. Jones. IEEE Trans. Sonics and Ultrasonics, SU15 No. 4, 209, (1968).
- [20] G. R. Aizin and G. Gumbs. Phys. Rev. B, **58**, 10589, (1998).
- [21] G. Gumbs and G. R. Aizin. Phys. Rev. B, **60**, 954, (1999).
- [22] A. Preumont. Vibration Control of Active Structures - An Introduction. Kluwer Academic Publishers, (1997).
- [23] H. P. Langtangen. *Computational Partial Differential Equations – Numerical Methods and Diffpack Programming*. Text in Computational Science and Engineering, vol 1. Springer, 2nd edition, (2003).
- [24] O. Zienkiewicz. The Finite Element Method. McGraw-Hill, 4th edition, (1994).
- [25] A. Iserles, *A first course in the numerical analysis of differential equations*, Cambridge University Press, (1995).
- [26] H. P. Langtangen. International Journal of Numerical Methods in Fluids, **10**, 213, (1989).
- [27] R. D. Cook, D. S. Malkus, and M. E. Plesha. Concepts and Applications of Finite Element Analysis. Wiley, 3rd edition, (1989).
- [28] H. P. Langtangen and O. Munthe. ACM Transactions on Mathematical Software, **27**, 1, March (2001).
- [29] O. Munthe and H. P. Langtangen. Computer Methods in Applied Mechanics and Engineering, **190**, 865, (2000).
- [30] S. H. Simon, Phys. Rev. B **54**, 13878 (1996).

A finite element method for modelling electromechanical wave propagation in anisotropic piezoelectric media

S. Rahman^{1,*}, H. P. Langtangen², and C. H. W. Barnes¹

¹*Cavendish Laboratory, Cambridge University, J J Thomson Avenue, Cambridge, CB3 0HE, United Kingdom and*

²*Simula Research Laboratory, Martin Linges v 17, Fornebu P.O.Box 134, 1325 Lysaker, Norway*

We describe and evaluate a numerical solution strategy for simulating surface acoustic waves (SAWs) through semiconductor devices with complex geometries. This multi-physics problem is of particular relevance to the design of SAW-based quantum electronic devices. The mathematical model consists of two coupled partial differential equations for the elastic wave propagation and the electric field, respectively, in anisotropic piezoelectric media. These equations are discretized by the finite element method in space and by a finite difference method in time. The latter method yields a convenient numerical decoupling of the governing equations. We describe how a computer implementation can utilize the decoupling and, via object-oriented programming techniques reuse independent codes for the Poisson equation and the linear time-dependent elasticity equation. First we apply the simulator to a simplified model problem for verifying the implementation, and thereafter we show that the methodology is capable of simulating a real-world case from nanotechnology, involving SAWs in a geometrically non-trivial device made of Gallium Arsenide.

PACS numbers: 02.70.Dc, 85.35.Gv, 73.23.-b, 77.65.Dq, 02.60.x

I. INTRODUCTION

In the process of designing quantum electronic devices based on surface acoustic waves (SAWs) traversing piezoelectric media, it is necessary to determine the effect, on these waves of obstacles such as electrical gates on the surface, and also the effect of the SAW on the low-dimensional quantum mechanical systems such as quantum wires and quantum dots. In general, the gates have a non-trivial geometry, which necessitate numerical simulation tools. The finite element method is well suited to handle complex geometries and is widely used to model piezoelectric devices [1, 2, 3, 4, 5, 6]. The effect on the low-dimensional quantum mechanical systems would be analyzed through coupling the SAW simulator to both stationary and time-dependent Schrödinger equations [7]. This would require the development of a fast SAW simulator but also flexible and portable code.

SAWs are modes of propagation of energy along the free surface of a material such that there is no decay along the direction of propagation but there is exponential decay into the bulk. SAWs have been used in electrical sensor technologies for many decades and have also been a useful tool in probing quantum electronic structures, for example, quantum Hall liquids [8]. Recently, much experimental work has been done in the field of acoustic charge transport whereby a SAW across a GaAs/AlGaAs heterostructure is used to capture a single electron and then transport it along a one-dimensional quantum wire [9]. This would be useful in developing an accurate cur-

rent standard, but more challenging proposals to use this in the burgeoning field of quantum information processing have been proposed [10, 11, 12, 13, 14]. SAWs have also been utilized for both static quantum dot [15] and photo-luminescence experiments [16, 17]. The time and resources required to build such devices are immense, and therefore the mathematical modelling of these devices before the physical construction is advantageous. This approach requires the solution of the continuum electromechanical equations of motion in a piezoelectric medium. The method of partial waves [18] can be used to obtain simple analytical expressions for the waves in the bulk material, but the solutions say nothing about the effect of gates on the surface. Attempts to solve the governing equations analytically for devices which do have surface gates [19, 20, 21] involve simplifications, and the accuracy of these approximations remains uncertain.

There is a vast amount of literature on the three-dimensional finite element analysis of piezoelectric devices [1, 2, 3, 4, 5, 6], and these methods are exploited in the field of ultrasonics to design control systems involving piezoelectric actuators and sensors [22]. Commercial software such as ANSYS and ABAQUS can be used to simulate electromechanical phenomena but lack the flexibility to couple to quantum mechanical calculations such as iterative Poisson-Schrödinger [7]. Therefore it is often necessary to develop one's own computer code for modelling such devices.

In this paper, we formulate and evaluate a finite element based solution method for the equations governing SAWs in piezoelectric media, and we formulate it in a flexible and portable manner to allow the ability to interface with other code. The implementation is performed in an object-oriented style in order to incorporate existing solvers and to enhance portability of the code. Such a tool can be valuable in the design of micro- and nano-scale devices. We describe a set of boundary conditions

*Electronic address: S.Rahman.00@cantab.net

that are capable of efficiently exciting SAWs and demonstrate the propagation of SAWs through a GaAs-based device. Although our applications are specific to GaAs, the formulation is general enough to allow simulations, with the same code (or with small modifications), of any crystal structure provided the elastic and piezoelectric material parameters are known.

This paper is organized as follows. In Section II we give an overview of the mathematical model underlying piezoelectricity and precisely state the coupled partial differential equations we aim to solve. Sections III and IV concern finite element formulations of these equations and an overview of the computational algorithm is described. In section V we describe the class based simulator approach used in our code design which simplifies implementation and increases reliability. Section VI presents a verification of the implementation and an empirical estimation of convergence properties of the numerical solution method. A real-world application of the methodology, concerning a SAW problem in nanotechnology is the subject of Section VII, before we make some concluding remarks in the final section.

II. MODELLING OF PIEZOELECTRIC MATERIALS

For piezoelectric materials, the electric displacement depends on both the applied electric field and mechanical strain, and the stresses depend on both the applied mechanical strain and applied electric field. The electric displacement D_i is given by

$$D_i = \epsilon_{ij}^S E_j + e_{ijk} \varepsilon_{jk}, \quad (1)$$

where E_j denotes the electric field, ϵ_{ij} is the permittivity tensor, e_{ijk} is the piezoelectric coupling constant, ε_{ij} is the strain tensor. The stress tensor σ_{ij} is given by

$$\sigma_{ij} = -e_{kij} E_k + c_{ijkl}^E \varepsilon_{kl}, \quad (2)$$

where c_{ijkl} represents the 4th rank tensor of elastic parameters. Summation over repeated indices is implied in this section, and the superscripts S and E denote that the quantities were measured under constant strain and constant electric field, respectively.

In the absence of free charges within the material, Gauss's law requires the divergence of the electric displacement to vanish:

$$\nabla \cdot D = \varrho_{\text{free}} = 0. \quad (3)$$

Combining Eqs. (1) and (2), and the relation

$$E_i = -\frac{\partial \phi}{\partial x_i} \quad (4)$$

between the electric potential ϕ and the electric field E_i , together with the strain-displacement relation for small strains,

$$\varepsilon_{ij} = \frac{1}{2} \left(\frac{\partial u_j}{\partial x_i} + \frac{\partial u_i}{\partial x_j} \right), \quad (5)$$

where u_i is the mechanical displacement field, we can derive a scalar partial differential equation for ϕ :

$$\frac{\partial}{\partial x_i} \epsilon_{ik}^S \frac{\partial \phi}{\partial x_k} = \frac{\partial}{\partial x_i} e_{ikl} \frac{\partial u_l}{\partial x_k}. \quad (6)$$

This equation couples the potential ϕ and the displacements u_i in the medium, and can be used to compute the electric field. Equation (4) assumes the quasi-static approximation, which requires that very little energy is carried away by electromagnetic waves.

The displacement field in the medium is governed by Newton's 2nd law of motion combined with the appropriate constitutive law. The former equation reads

$$\varrho \ddot{u}_i = \frac{\partial \sigma_{ij}}{\partial x_j} + \varrho b_i, \quad (7)$$

where b_i denotes body forces, and the double dot in \ddot{u}_i denotes a second-order partial derivative in time. As Eq. (7) stands, it contains no damping term, which is irrelevant in our application setting. The constitutive law stated in Eq. (2) relates the stress tensor σ_{ij} to the strain tensor ε_{ij} , and Eq. (5) relates ε_{ij} to the displacement field u_i . Combining Eqs. (2), (5), (7), we arrive at an equation for u_i in terms of ϕ :

$$\varrho \ddot{u}_i = \frac{\partial}{\partial x_j} c_{ijkl}^E \frac{\partial u_l}{\partial x_k} + \varrho b_i + \frac{\partial}{\partial x_j} e_{kij} \frac{\partial \phi}{\partial x_k}. \quad (8)$$

From Eq. (8) we see how the mechanical motion is affected the electric field. In most materials, this coupling is weak, because $e_{ijk} \ll c_{ijkl}^E$, and the effect of the piezoelectric potential on the mechanical deformation is negligible. On the other hand, the effect of the mechanical deformation on the potential is always significant according to Eq. (6). However, in cases where an external electric field is applied through surface gates, the term in ϕ may be sufficiently large to contribute significantly to the mechanical motion, and these cases receive the focus of the present paper.

To illustrate the nature of these equations we explicitly write out the coupling terms for the piezoelectric material GaAs. The elastic parameters of a crystal are usually given in a coordinate system with its x , y and z axes parallel to the crystal X, Y and Z axes. For consistency with acoustoelectric charge transport experiments, we align the positive x axis with the crystal positive [011] axes, and the positive z axis with the crystal positive [100] axis. To achieve this we perform a 45 degree rotation of the crystal, around the z axis.

In the transformed frame, the only non-zero components of the piezoelectric tensor are $e_{15} = -e_{24} = e_{31} = -e_{32}$. For generality, we illustrate our method using the different values of the piezoelectric tensor. Using the as-

sumptions stated in the previous paragraph, and neglecting body forces, we can write out equations Eqs. (8) and (6) as

$$\rho \ddot{u}_x = \frac{\partial}{\partial x_j} c_{xjkl}^E \frac{\partial u_l}{\partial x_k} + \frac{\partial}{\partial x} e_{31} \frac{\partial \phi}{\partial z} + \frac{\partial}{\partial z} e_{15} \frac{\partial \phi}{\partial x}, \quad (9)$$

$$\rho \ddot{u}_y = \frac{\partial}{\partial x_j} c_{yjkl}^E \frac{\partial u_l}{\partial x_k} + \frac{\partial}{\partial y} e_{32} \frac{\partial \phi}{\partial z} + \frac{\partial}{\partial z} e_{24} \frac{\partial \phi}{\partial y}, \quad (10)$$

$$\rho \ddot{u}_z = \frac{\partial}{\partial x_j} c_{zjkl}^E \frac{\partial u_l}{\partial x_k} + \frac{\partial}{\partial x} e_{15} \frac{\partial \phi}{\partial x} + \frac{\partial}{\partial y} e_{24} \frac{\partial \phi}{\partial y}, \quad (11)$$

$$\nabla \cdot \epsilon_s^S \nabla \phi = \frac{\partial}{\partial x} e_{15} \frac{\partial u_z}{\partial x} + \frac{\partial}{\partial y} e_{24} \frac{\partial u_z}{\partial y} + \frac{\partial}{\partial z} e_{31} \frac{\partial u_x}{\partial x} + \frac{\partial}{\partial x} e_{15} \frac{\partial u_x}{\partial z} + \frac{\partial}{\partial z} e_{32} \frac{\partial u_y}{\partial y} + \frac{\partial}{\partial y} e_{24} \frac{\partial u_y}{\partial z}. \quad (12)$$

In Refs. (20) and (21) analytical solutions of these equations were obtained, under the assumption that the ϕ term in Eqs. (9)–(11) can be ignored. This means that the mechanical motion is decoupled from the electric field, but an electric field is induced from the mechanical motion. The reliability of such substantial simplifications

is limited to cases where the external potential ϕ is small. Also, the obtained solutions are for two-dimensional cases only and are therefore of minor interest when studying the effect of surface gates. Solving the fully coupled system of PDEs demands numerical techniques like the one described in the next section.

III. FINITE ELEMENT FORMULATION

We shall use the finite element method in space and the finite difference method in time. The reasons for applying the finite element method are the need for handling geometrically complicated domains and the fact that the method works very well for elasticity problems without coupling to ϕ as well as for the Poisson equation for ϕ .

We point out that the finite element formulation presented in this paper is independent of the choice of element shape, as this would be problem dependent. The elasticity part of the problem has three degrees of freedom - one for each component of the displacement vector. The electrical part has one degree of freedom for the electric potential.

A. The Poisson equation with piezoelectric coupling

Before continuing further, it is convenient to introduce a superscript ℓ to denote the time level, for example, ϕ^ℓ is ϕ at time level ℓ . The electrostatic potential ϕ^ℓ due to mechanical displacements u_i^ℓ in the piezoelectric material concerned is given by Eq. (12). The finite element formulation of such a Poisson equation is well covered in the literature [7, 23, 24, 25]. The basic idea is to approximate ϕ^ℓ by a linear combination of basis functions N_i , $\phi^\ell \approx \hat{\phi}^\ell = \sum_{j=1}^n N_j \phi_j^\ell$, insert $\hat{\phi}^\ell$ in the Poisson equation, and demand the residual to be orthogonal to the space spanned by $\{N_1, \dots, N_n\}$. The Laplace term is integrated by parts.

The only non-trivial aspect of the formulation in the present setting is the right-hand side, where the second-order derivatives of the elastic field demand integration by parts. The two first terms on the right-hand side of Eq. (12) give rise to an integral, which is straightforwardly integrated as

$$\begin{aligned} & - \int_{\Omega} N_i \left[\frac{\partial}{\partial x} e_{15} \frac{\partial u_z^\ell}{\partial x} + \frac{\partial}{\partial y} e_{24} \frac{\partial u_z^\ell}{\partial y} \right] d\Omega \\ & = \int_{\Omega} \left[e_{15} \frac{\partial N_i}{\partial x} \frac{\partial u_z^\ell}{\partial x} + e_{24} \frac{\partial N_i}{\partial y} \frac{\partial u_z^\ell}{\partial y} \right] d\Omega - \oint_{\partial\Omega} N_i \left[e_{15} \frac{\partial u_z^\ell}{\partial x} n_x + e_{24} \frac{\partial u_z^\ell}{\partial y} n_y \right] d\Gamma. \end{aligned} \quad (13)$$

The terms in Eq. (12), containing mixed derivatives, can be integrated by parts using a special form of Green's Theorem,

$$-\int_{\Omega} \phi \frac{\partial \psi}{\partial z} dx dy dz = \int_{\Omega} \frac{\partial \phi}{\partial z} \psi dx dy dz - \oint_{\Gamma} \phi \psi n_z d\Gamma. \quad (14)$$

The terms give rise to the integrals

$$\begin{aligned} & -\int_{\Omega} N_i \left[\frac{\partial}{\partial z} e_{31} \frac{\partial u_x^\ell}{\partial x} + \frac{\partial}{\partial x} e_{15} \frac{\partial u_x^\ell}{\partial z} + \frac{\partial}{\partial z} e_{32} \frac{\partial u_y^\ell}{\partial y} + \frac{\partial}{\partial y} e_{24} \frac{\partial u_y^\ell}{\partial z} \right] d\Omega \\ & = \int_{\Omega} \left[e_{31} \frac{\partial N_i}{\partial z} \frac{\partial u_x^\ell}{\partial x} + e_{15} \frac{\partial N_i}{\partial x} \frac{\partial u_x^\ell}{\partial z} + e_{32} \frac{\partial N_i}{\partial z} \frac{\partial u_y^\ell}{\partial y} + e_{24} \frac{\partial N_i}{\partial y} \frac{\partial u_y^\ell}{\partial z} \right] d\Omega \\ & - \oint_{\partial\Omega} N_i \left[e_{31} \frac{\partial u_x^\ell}{\partial x} n_z + e_{15} \frac{\partial u_x^\ell}{\partial z} n_x + e_{32} \frac{\partial u_y^\ell}{\partial y} n_z + e_{24} \frac{\partial u_y^\ell}{\partial z} n_y \right] d\Gamma. \end{aligned} \quad (15)$$

The finite element method applied to the equation for ϕ transforms the PDE problem to a linear system of equations,

$$\mathbf{P}\boldsymbol{\phi}^\ell = \mathbf{f}^\ell, \quad (16)$$

where the ‘stiffness’ matrix \mathbf{P} has its (i, j) element given by

$$P_{ij} = \int_{\Omega} \epsilon_s^S \left[\frac{\partial N_i}{\partial x} \frac{\partial N_j}{\partial x} + \frac{\partial N_i}{\partial y} \frac{\partial N_j}{\partial y} + \frac{\partial N_i}{\partial z} \frac{\partial N_j}{\partial z} \right] d\Omega. \quad (17)$$

The $\boldsymbol{\phi}^\ell$ vector in Eq. (16) contains the values of ϕ^ℓ at the nodal points. The i -th component f_i^ℓ of the right-hand side vector \mathbf{f}^ℓ can be written as

$$f_i^\ell = \oint_{\partial\Omega} \epsilon_s^S N_i \frac{\partial \phi^\ell}{\partial n} d\Gamma - \oint_{\partial\Omega} N_i r d\Gamma + \int_{\Omega} s d\Omega, \quad (18)$$

with

$$\begin{aligned} r &= e_{31} \frac{\partial u_x^\ell}{\partial x} n_z + e_{15} \frac{\partial u_x^\ell}{\partial z} n_x + e_{32} \frac{\partial u_y^\ell}{\partial y} n_z + e_{24} \frac{\partial u_y^\ell}{\partial z} n_y + e_{15} \frac{\partial u_z^\ell}{\partial x} n_x + e_{24} \frac{\partial u_z^\ell}{\partial y} n_y, \\ s &= e_{31} \frac{\partial N_i}{\partial z} \frac{\partial u_x^\ell}{\partial x} + e_{15} \frac{\partial N_i}{\partial x} \frac{\partial u_x^\ell}{\partial z} + e_{32} \frac{\partial N_i}{\partial z} \frac{\partial u_y^\ell}{\partial y} + e_{24} \frac{\partial N_i}{\partial y} \frac{\partial u_y^\ell}{\partial z} + e_{15} \frac{\partial N_i}{\partial x} \frac{\partial u_z^\ell}{\partial x} + e_{24} \frac{\partial N_i}{\partial y} \frac{\partial u_z^\ell}{\partial y}. \end{aligned}$$

When the displacement field entering f_i^ℓ is known, any standard Poisson solver can be used to compute $\boldsymbol{\phi}^\ell$.

B. The elasticity problem with electric field loading

For the finite element formulation of Eq. (8) it is easier to first start with Eq. (7) and insert the constitutive law given by Eq. (2) and the strain-displacement relation given by Eq. (5) in the finite element integrals. The time derivative in Eq. (8) can be approximated by a second-order accurate finite difference. Sampling Eq. (8) at time level ℓ then yields

$$\varrho \frac{u_i^{\ell-1} - 2u_i^\ell + u_i^{\ell+1}}{\Delta t^2} = \frac{\partial \sigma_{ij}^\ell}{\partial x_j} + \varrho b_i^\ell, \quad (19)$$

where Δt is the time step length and quantities with the ℓ superscript are functions of space only. This time discretization introduces an operator splitting such that the originally coupled governing equations can be solved in

sequence. No accuracy is lost by this operator splitting beyond that implied by the finite difference itself in Eq. (19). More precisely, σ_{ij}^ℓ contains ϕ^ℓ , which is known, such that we can easily solve for $u_i^{\ell+1}$ using old values of ϕ . On the next time level $(\ell + 1)$, we can find $\phi^{\ell+1}$ using the recently computed $u_i^{\ell+1}$.

The main motivation for the explicit time differencing in Eq. (19) is numerical efficiency: (i) we decouple the equations, which simplifies the numerics and the implementation, and (ii) there is no need to solve large sparse linear systems of equations in the elasticity part of the problem (if the mass matrix is lumped). Nevertheless, the time difference Eq. (19) leads to a conditionally stable scheme, where Δt must be of the order of the smallest element size. In wave propagation problems, uniform high resolution is frequently needed in space and time, typically compatible with the stability restriction, which makes such explicit schemes appropriate. On the other hand, in applications where adaptive grids with great variation in element size are needed, one may benefit from implicit schemes (for example, of Newmark type) [24].

The finite element formulation of Eq. (19) is easiest to express if we switch to a typical “finite element engineering” notation, especially when we deal with anisotropic media. The stress and strain tensors are expressed as vectors,

$$\begin{aligned}\boldsymbol{\sigma} &= (\sigma_{xx}, \sigma_{yy}, \sigma_{zz}, \sigma_{yz}, \sigma_{zx}, \sigma_{yx})^T, \\ \boldsymbol{\varepsilon} &= (\varepsilon_{xx}, \varepsilon_{yy}, \varepsilon_{zz}, 2\varepsilon_{yz}, 2\varepsilon_{zx}, 2\varepsilon_{yx})^T.\end{aligned}$$

The constitutive law can then be written as

$$\boldsymbol{\sigma}^\ell = \mathbf{D}\boldsymbol{\varepsilon}^\ell + \mathbf{p}^\ell, \quad (20)$$

where the \mathbf{p}^ℓ term represents the loading from the electric field, and \mathbf{D} is a symmetric 6×6 matrix of the elasticity coefficients (previously denoted by c_{ijkl}^E):

$$\mathbf{D} = \begin{bmatrix} c_{11} & c_{12} & c_{13} & c_{14} & c_{15} & c_{16} \\ & c_{12} & c_{13} & c_{14} & c_{15} & c_{16} \\ & & c_{13} & c_{14} & c_{15} & c_{16} \\ & & & c_{14} & c_{15} & c_{16} \\ & & & & c_{15} & c_{16} \\ & & & & & c_{16} \end{bmatrix}. \quad (21)$$

The displacement field at a time level ℓ is approximated according to

$$u_i^\ell \approx \hat{\mathbf{u}}^\ell = \sum_{j=1}^n N_j \mathbf{u}_j^\ell,$$

where \mathbf{u}_j^ℓ is the value of the displacement field at node j at time level ℓ . The strain-displacement relation then becomes

$$\boldsymbol{\varepsilon}^\ell = \sum_{j=1}^n \mathbf{B}_j \mathbf{u}_j^\ell, \quad \mathbf{B}_i = \begin{bmatrix} N_{i,x} & 0 & 0 \\ 0 & N_{i,y} & 0 \\ 0 & 0 & N_{i,z} \\ 0 & N_{i,z} & N_{i,y} \\ N_{i,z} & 0 & N_{i,x} \\ N_{i,y} & N_{i,x} & 0 \end{bmatrix}. \quad (22)$$

The comma notation here denotes partial derivative: $N_{i,x} \equiv \partial N_i / \partial x$.

A finite element formulation of Eq. (19) using the aforementioned notation becomes (see Ref. 23 for a detailed derivation without the ϕ term)

$$\int_{\Omega} \varrho N_i \sum_{j=1}^n N_j (\mathbf{u}_j^{\ell-1} - 2\mathbf{u}_j^\ell + \mathbf{u}_j^{\ell+1}) d\Omega + \Delta t^2 \int_{\Omega} \mathbf{B}_i^T \boldsymbol{\sigma}^\ell d\Omega = \Delta t^2 \int_{\Omega} \varrho \mathbf{b} N_i d\Omega + \Delta t^2 \int_{\partial\Omega} \mathbf{t}^\ell N_i d\Gamma. \quad (23)$$

Here, \mathbf{t}^ℓ is the traction on the boundary, arising from integrating the divergence of the stress in Eq. (19) by parts. Inserting the constitutive law in the term $\int_{\Omega} \mathbf{B}_i^T \boldsymbol{\sigma} d\Omega$ yields

$$\sum_{j=1}^n \left(\int_{\Omega} \mathbf{B}_i^T D \mathbf{B}_j d\Omega \right) \mathbf{u}_j^\ell + \int_{\Omega} \mathbf{B}_i^T \mathbf{p}^\ell d\Omega.$$

The final discrete equations arising from the equation of motion can be written as

$$\mathbf{u}^{\ell+1} = 2\mathbf{u}^\ell - \mathbf{u}^{\ell-1} + \Delta t^2 \tilde{\mathbf{M}}^{-1} (-\mathbf{K} \mathbf{u}^\ell + \boldsymbol{\beta}^\ell + \boldsymbol{\Phi}^\ell), \quad (24)$$

where $\tilde{\mathbf{M}}^{-1}$ is an efficient inverse of the mass matrix \mathbf{M} resulting from the $\int_{\Omega} \rho N_i N_j d\Omega$ integral. We construct $\tilde{\mathbf{M}}^{-1}$ as the inverse of the lumped mass matrix (using the row-sum technique to lump the matrix). The matrix \mathbf{K} stems from the standard “stiffness” term $\int_{\Omega} \mathbf{B}_i^T D \mathbf{B}_j d\Omega$ representing anisotropic elasticity, $\boldsymbol{\beta}^\ell$ is the effect of body forces and surface tractions, and $\boldsymbol{\Phi}^\ell$ is the contribution from the electric field. The i -th block (arising from node i) in $\boldsymbol{\Phi}^\ell$ takes the form $\boldsymbol{\Phi}_i^\ell = \int_{\Omega} \mathbf{B}_i^T \mathbf{p}^\ell$, which from Eqs. (9) to (11) results in

$$\boldsymbol{\Phi}_i^\ell = \begin{bmatrix} \int_{\Omega} N_i \left[\frac{\partial}{\partial x} e_{31} \frac{\partial \phi^\ell}{\partial z} + \frac{\partial}{\partial z} e_{15} \frac{\partial \phi^\ell}{\partial x} \right] d\Omega \\ - \int_{\Omega} N_i \left[\frac{\partial}{\partial y} e_{32} \frac{\partial \phi^\ell}{\partial z} + \frac{\partial}{\partial z} e_{24} \frac{\partial \phi^\ell}{\partial y} \right] d\Omega \\ \int_{\Omega} N_i \left[\frac{\partial}{\partial x} e_{15} \frac{\partial \phi^\ell}{\partial x} + \frac{\partial}{\partial y} e_{24} \frac{\partial \phi^\ell}{\partial y} \right] d\Omega \end{bmatrix}$$

$$= \begin{bmatrix} - \int_{\Omega} \left[e_{31} \frac{\partial N_i}{\partial x} \frac{\partial \phi^\ell}{\partial z} + e_{15} \frac{\partial N_i}{\partial z} \frac{\partial \phi^\ell}{\partial x} \right] d\Omega + \int_{\partial\Omega} N_i \left[e_{31} \frac{\partial \phi^\ell}{\partial z} n_x + e_{15} \frac{\partial \phi^\ell}{\partial x} n_z \right] d\Gamma \\ \int_{\Omega} \left[e_{32} \frac{\partial N_i}{\partial y} \frac{\partial \phi^\ell}{\partial z} + e_{24} \frac{\partial N_i}{\partial z} \frac{\partial \phi^\ell}{\partial y} \right] d\Omega - \int_{\partial\Omega} N_i \left[e_{32} \frac{\partial \phi^\ell}{\partial z} n_y + e_{24} \frac{\partial \phi^\ell}{\partial y} n_z \right] d\Gamma \\ - \int_{\Omega} \left[e_{15} \frac{\partial N_i}{\partial x} \frac{\partial \phi^\ell}{\partial x} + e_{24} \frac{\partial N_i}{\partial y} \frac{\partial \phi^\ell}{\partial y} \right] d\Omega + \int_{\partial\Omega} N_i \left[e_{15} \frac{\partial \phi^\ell}{\partial x} n_x + e_{24} \frac{\partial \phi^\ell}{\partial y} n_y \right] d\Gamma \end{bmatrix}. \quad (25)$$

Our governing equations require initial conditions. Let us assume that the elastic body is at rest such that $\partial u_i / \partial t = 0$. The external electric field is then turned on. After the initial transients the displacement field have faded out, and we have a stationary initial state of our system, modeled by the equations

$$\mathbf{P} \boldsymbol{\phi}^0 = \mathbf{f}^0(\mathbf{u}^0), \quad (26)$$

$$\mathbf{K} \mathbf{u}^0 = \boldsymbol{\beta}^0 + \boldsymbol{\Phi}^0(\boldsymbol{\phi}^0). \quad (27)$$

These two coupled equations are solved by an iterative Gauss-Seidel-like technique, i.e., the equations are solved one at a time, using the most recent approximation of the other field in the right-hand side term. Each linear system is solved by a MILU preconditioned conjugate gradient method [26]. The solution of Eqs. (26) and (27), along with the assumption of stationarity, $\partial \mathbf{u} / \partial t = 0$, comprise the initial condition.

As boundary conditions, we either have prescribed traction components or prescribed displacement components, along with prescribed electric potential or prescribed normal component of the electric field. The displacement equation needs three boundary conditions at each point at the boundary, while the equation for ϕ needs one condition at each point.

From $\partial \mathbf{u} / \partial t = 0$ at $t = 0$ it follows by a second-order difference approximation that $\mathbf{u}^1 = \mathbf{u}^{-1}$. From Eqs. (24) and (27) it follows that $\mathbf{u}^1 = \mathbf{u}^0 = \mathbf{u}^{-1}$. The loads removed at $t = 0^+$ will first come into play at the second time level.

The computational algorithm can now be formulated as follows:

$\ell = 0$ (time level counter)
 $k = 0$ (iteration counter)
 while $\varepsilon < \varepsilon_{crit}$
 solve Eq. (26) w.r.t $\boldsymbol{\phi}^{0,k}$

solve Eq. (27) w.r.t $\mathbf{u}^{0,k}$
 compute $\varepsilon = \|\mathbf{u}^{0,k} - \mathbf{u}^{0,k-1}\| + \|\phi^{0,k} - \phi^{0,k-1}\|$
 $k \leftarrow k + 1$ end while
 $\phi^1 = \phi^0, \mathbf{u}^1 = \mathbf{u}^0$
 for $\ell = 1, 2, 3, \dots$ until end of simulation
 solve Eq. (24) w.r.t $\mathbf{u}^{\ell+1}$
 solve Eq. (16) w.r.t $\phi^{\ell+1}$

Comments on Stability. The stability criterion of the explicit finite difference scheme in time, when decoupled from the electric field problem, requires $\Delta t \leq 2/\omega_{\max}$ [27], where ω_{\max} is the highest natural frequency of the vibrating system. One may find ω_{\max} as the square root of the largest eigenvalue of the problem $\mathbf{K} - \lambda\mathbf{M} = 0$. An approximate bound on ω_{\max} can be estimated from a relation $\omega_{\max} = 2c/h_{\text{eff}}$, where c is the speed of elastic waves and h_{eff} is the smallest effective element length. The stability criterion now reduces to the common Courant, Friedrichs, and Lewy (CFL) condition:

$$\Delta t \leq \alpha h_{\text{eff}}/c. \quad (28)$$

Here, α is a factor to be adjusted since the h_{eff} parameter is normally roughly computed from element sizes or application of Gerschgorin's theorem applied to the underlying eigenvalue problem. For wave problems the CFL condition is frequently not particularly restrictive since the length and period of a wave are usually proportional, leading to a natural choice of $\Delta t/h = \text{const.}$

IV. AN OPTIMISED FINITE ELEMENT FORMULATION

We can speed up the numerical computation by replacing the complete assembly of the right-hand side vectors in Eqs. (16) and (24) by a matrix-vector product. For example, consider the contribution to the vector \mathbf{f} in Eq. (16) due to the coupling from the mechanical motion (omitting the superscript ℓ for the remainder of this section):

$$\int_{\Omega} e_{31} \frac{\partial N_i}{\partial z} \frac{\partial u_x}{\partial x} + e_{15} \frac{\partial N_i}{\partial x} \frac{\partial u_x}{\partial z} + e_{32} \frac{\partial N_i}{\partial z} \frac{\partial u_y}{\partial y} + e_{24} \frac{\partial N_i}{\partial y} \frac{\partial u_y}{\partial z} + e_{15} \frac{\partial N_i}{\partial x} \frac{\partial u_z}{\partial x} + e_{24} \frac{\partial N_i}{\partial y} \frac{\partial u_z}{\partial y} d\Omega. \quad (29)$$

Inserting the finite element expansion $u_x \approx \sum_{j=1}^n u_j^{(x)} N_j$, and similar expansions for u_y and u_z , the expression in Eq. (29) results in

$$\begin{aligned} & \sum_{j=1}^n \int_{\Omega} e_{31} \frac{\partial N_i}{\partial z} \frac{\partial N_j}{\partial x} u_j^{(x)} + e_{15} \frac{\partial N_i}{\partial x} \frac{\partial N_j}{\partial z} u_j^{(x)} + e_{32} \frac{\partial N_i}{\partial z} \frac{\partial N_j}{\partial y} u_j^{(y)} \\ & + e_{24} \frac{\partial N_i}{\partial y} \frac{\partial N_j}{\partial z} u_j^{(y)} + e_{15} \frac{\partial N_i}{\partial x} \frac{\partial N_j}{\partial x} u_j^{(z)} + e_{24} \frac{\partial N_i}{\partial y} \frac{\partial N_j}{\partial y} u_j^{(z)} d\Omega. \end{aligned} \quad (30)$$

This expression can be written as a matrix vector product $\mathbf{L}\mathbf{u}$, where the matrix \mathbf{L} consists of $n \times n$ blocks, each block of size 1×3 . For the coupling of node i and j , the 3×1 block looks like

$$e_{31} \frac{\partial N_i}{\partial z} \frac{\partial N_j}{\partial x} + e_{15} \frac{\partial N_i}{\partial x} \frac{\partial N_j}{\partial z}, e_{32} \frac{\partial N_i}{\partial z} \frac{\partial N_j}{\partial y} + e_{24} \frac{\partial N_i}{\partial y} \frac{\partial N_j}{\partial z}, e_{15} \frac{\partial N_i}{\partial x} \frac{\partial N_j}{\partial x} + e_{24} \frac{\partial N_i}{\partial y} \frac{\partial N_j}{\partial y}, \quad (31)$$

The Poisson equation - Eq. (16) for ϕ can now be written as

$$\mathbf{P}\phi^{\ell+1} = \mathbf{L}\mathbf{u}^{\ell+1}. \quad (32)$$

At each time level we can hence avoid the costly finite element assembly process, since \mathbf{P} and \mathbf{L} are constant in time and the right-hand side of the linear system is obtained by an efficient matrix-vector product. This may result in a significant speed-up of the solver. For large number of unknowns, the speed up is experienced only if we use a method of complexity or order n , like multigrid, to solve Eq. (32).

Equation (24) is already on a favorable matrix-vector algebra form, except for the coupling term Φ^ℓ . Examining Eq. (25), we realize that this matrix can be written as $\Phi^\ell = \mathbf{Q}\phi^\ell$, where \mathbf{Q} is a time-independent $n \times n$ matrix of 3×1 blocks. The contribution to block i in Φ^ℓ is made of the coupling \mathbf{Q}_{ij} between node i and j and the block j in ϕ^ℓ : $\Phi_i^\ell = \mathbf{Q}_{ij}\phi_j^\ell$, where

$$\mathbf{Q}_{ij} = \begin{bmatrix} -\int_{\Omega} e_{31} \frac{\partial N_i}{\partial x} \frac{\partial N_j}{\partial z} + e_{15} \frac{\partial N_i}{\partial z} \frac{\partial N_j}{\partial x} d\Omega + \int_{\partial\Omega} N_i [e_{31} \frac{\partial N_j}{\partial z} n_x + e_{15} \frac{\partial N_j}{\partial x} n_z] d\Gamma \\ \int_{\Omega} e_{32} \frac{\partial N_i}{\partial y} \frac{\partial N_j}{\partial z} + e_{24} \frac{\partial N_i}{\partial z} \frac{\partial N_j}{\partial y} d\Omega - \int_{\partial\Omega} N_i [e_{32} \frac{\partial N_j}{\partial z} n_y + e_{24} \frac{\partial N_j}{\partial y} n_z] d\Gamma \\ -\int_{\Omega} e_{15} \frac{\partial N_i}{\partial x} \frac{\partial N_j}{\partial x} + e_{24} \frac{\partial N_i}{\partial y} \frac{\partial N_j}{\partial y} d\Omega + \int_{\partial\Omega} N_i [e_{15} \frac{\partial N_j}{\partial x} n_x + e_{24} \frac{\partial N_j}{\partial y} n_y] d\Gamma \end{bmatrix}.$$

Now the Φ^ℓ term in Eq. (24) can be computed as a matrix-vector product $\mathbf{Q}\phi^\ell$, and no assembly process is required to construct Eq. (24) at each time level. In our algorithm we must run assembly processes at $t = 0$ to construct the matrices $\tilde{\mathbf{M}}^{-1}$, \mathbf{K} , \mathbf{Q} , \mathbf{L} , and \mathbf{P} .

V. OBJECT-ORIENTED IMPLEMENTATION

A significant trend in modern software development is to formulate numerical algorithms such that reliable and well-tested software components can be combined together to form a new simulator. Our numerical approach was in particular inspired by such an approach. With the time discretization we were able to split the coupled u_i - ϕ system such that at each time level we first solve for a new displacement field (u_i) and then we solve for the corresponding electric potential (ϕ). In each of the two equations, the effect of the other only enters through a right-hand side “forcing” term. This allows us, in principle, to reuse a solver for elastic vibrations and a Poisson solver, as long as these solvers can implement a new right-hand side term that couples to another solver. From a principal point of view, this idea is simple and attractive. However, the implementation of the idea in practice may be less feasible if the design of the underlying solvers is not sufficiently flexible.

To allow for building the compound u_i - ϕ solver from separate u_i and ϕ solvers we propose to apply principles from object-oriented programming. The time-dependent elasticity solver and the Poisson solver are realized as two independent objects, implemented via classes in C++. Actually, we have reused the `Poisson2` class from Ref. 23 as the Poisson solver, and the `ElasticVib1` class from Ref. 23 as the elastic vibration solver. The latter is a subclass of `Elasticity2`, a pure quasi time-dependent elasticity solver (without the acceleration term in the momentum equation). These classes are implemented using building blocks from the Diffpack library [23].

The `Poisson2` and `ElasticVib1` classes have no knowledge of each other. The only common feature is their design. This design is crucial for reuse of the classes to solve the coupled problem, but the design approach suggested for Diffpack solvers [23, 28, 29] has proven to be successful in this respect. Diffpack solvers are realized as classes containing objects for grids, scalar/vector fields, linear systems, etc. The coefficients in a PDE are

evaluated through virtual functions. When the solver is stand-alone, these virtual functions contain mathematical expressions or measured data, but when solvers are combined, the virtual functions are reimplemented in subclasses and connected to data in other solvers. This principle reflects the underlying mathematics: the coefficients in a single PDE are considered known, but in a system of PDEs, the coefficients typically couple to unknown quantities governed by the PDEs. The present coupled system is an example where the right-hand side in the Poisson equation couples to the primary unknown in the elastic vibration solver, while a right-hand side term in the elastic vibration solver couples to the primary unknown in the Poisson equation. When the solvers are used independently there are no such couplings.

Figure 1 shows an outline of the class design for the compound solver. From class `Poisson2` we derive a subclass `Poisson2_glue`, which reimplements the virtual function in `Poisson2` for evaluating the right-hand side in that equation. In this new function we need to compute an expression involving the displacement field available in the `ElasticVib1` class. A manager class, simply called `Manager`, holds pointers to all classes for the individual PDEs in the system of PDEs, and each PDE class holds a pointer to the manager class, thus enabling a two-way communication. With these pointers, we can connect data from any other solver class to the `Poisson2_glue` class. In the virtual function evaluating the right-hand side we can typically call `mng->elastic->u` to get a vector field object for u_i that we can evaluate at the current integration point. This object has support for evaluating derivatives of the field as well.

Similarly, we derive a subclass `ElasticVib1_glue` of `ElasticVib1`, add a pointer to the manager class, and override the virtual function for evaluating the right-hand side. Now we need to compute expressions involving ϕ , but this is easily accomplished by the pointers, e.g., `mng->poisson->u` if `u` is the name of the unknown scalar field in the `Poisson2` solver.

The “glue” classes `Poisson2_glue` and `ElasticVib1_glue`

are very small compared to the real solver classes they inherit from. A “glue” class typically needs about a page of code unless it adds additional computations. The manager class is a bit more comprehensive since it implements the overall solution algorithm, i.e., the time stepping and the calls to the independent solvers.

The benefit from using object-oriented programming in the way we have outlined is that the original well-tested Poisson and elastic vibration solvers can be reused in a system of PDEs without any modifications. The original solver classes reside in separate files and are hence not subject to any side effects from editing the source code. The “glue” class is also in a separate file and enables the original solver to speak to a manager in charge of solving a compound system of PDEs. The advantages are clear: reliability is increased by reusing well-tested solvers, and the compound solver is modularized. Our experience is that this design reduces the development time significantly. Especially the debugging phase is greatly simplified. At any time, the underlying solvers can be trivially pulled out of the compound system and verified independently.

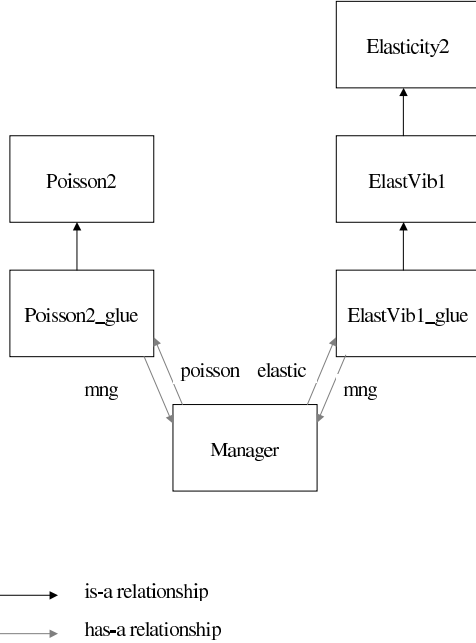


FIG. 1: Relationships between classes. The base classes, `Poisson2` and `Elasticity2` perform the solution of the standard time-independent Poisson and elasticity equations, respectively. `ElasticVib1` is derived from `Elasticity2` and solves for time-dependent elastic motion. The classes `Poisson2_glue` and `ElasticVib1_glue` implement the coupling between the electrostatic and mechanical equations, and these classes are controlled by the `Manager` class.

VI. VERIFICATION

Before showing numerical results for a physically relevant application, we report on the estimated numerical

accuracy of the code, thereby establishing evidence for the correctness of the implementation. To investigate numerical errors, we compare numerical results with an exact solution. The exact solution is based on the assumption of a displacement field in z direction only, depending on x and t only. Physically, a normal traction is applied at all $x = \text{const}$ and $y = \text{const}$ boundaries to avoid displacements in the x and y directions, but in the code we implement this situation by essential boundary conditions $u_x = u_y = 0$. We also assume that $\phi = \phi(x, t)$ and that the material is isotropic. The governing equations then reduce to

$$\varrho \ddot{u}_z = \mu \frac{\partial^2 u_z}{\partial x^2} + e_{15} \frac{\partial^2 \phi}{\partial x^2}, \quad (33)$$

$$\epsilon_s \frac{\partial^2 \phi}{\partial x^2} = e_{15} \frac{\partial^2 u_z}{\partial x^2}. \quad (34)$$

These equations can be scaled to yield

$$\ddot{u}_z = \frac{\partial^2 u_z}{\partial x^2} + \alpha \frac{\partial^2 \phi}{\partial x^2}, \quad (35)$$

$$\frac{\partial^2 \phi}{\partial x^2} = \frac{\partial^2 u_z}{\partial x^2}. \quad (36)$$

The constant α is zero or unity corresponding to whether the elasticity problem couples to the electric field problem or not. (The three coefficients in the original system are scaled away by choosing an appropriate time scale, ϕ scale, and u_i scale.) One possible solution of Eqs. (35)–(36) reads

$$u_z(x, t) = \phi(x, t) = \cos(k\sqrt{1+\alpha}t) \sin(kx). \quad (37)$$

In our tests we choose Ω as a three-dimensional beam and $k = \frac{n\pi}{L}$, with n being an integer and L the length of the beam. The ends of the beam are then fixed.

Our verification procedure consists of estimating the convergence rate of the numerical method. A scalar error measure e is expected to behave like

$$e = Ah^r + B\Delta t^s,$$

where A and B are constants independent of the element size h and the time step Δt . From the involved approximations, we expect $s = 2$ and $r = 1 + q$, where q is the order of the polynomials in an element. In particular, for linear or trilinear elements, $r = 2$, and if h and Δt are chosen such that $h/\Delta t = \text{const}$, we see that $e \sim h^r$. From two successive experiments, (h_{i-1}, e_{i-1}) and (h_i, e_i) we may estimate a convergence rate r_i from

$$r_i = \frac{\ln e_i / e_{i-1}}{\ln h_i / h_{i-1}}.$$

We have investigated three error measures, given as different norms of the error field $E = u_z - \hat{u}_z$, where \hat{u}_z is the numerical solution and u_z is the exact solution:

$$\|E\|_{L^1(\Omega)} = \int_{\Omega} |E| d\Omega, \quad \|E\|_{L^2(\Omega)} = \left(\int_{\Omega} E^2 d\Omega \right)^{\frac{1}{2}}, \quad \|E\|_{L^\infty(\Omega)} = \sup(|E(\mathbf{x})|, \mathbf{x} \in \Omega).$$

Table I displays the values of the error norms and the associated estimates of the convergence rates r_i . As the grid spacing h and the time step Δt are reduced, the numerical solution converges to the exact solution with the expected rate of two. This provides evidence for the correctness of the implementation and indicates that our overall solution method, including the operator splitting, is of second order in time and space. The spatial convergence rate is expected to increase with the order of the polynomials used in the elements.

h	$\ E\ _{L^1}$	rates	$\ E\ _{L^2}$	rates	$\ E\ _{L^\infty}$	rates
0.05	$2.440 \cdot 10^{-5}$		$2.710 \cdot 10^{-6}$		$3.830 \cdot 10^{-7}$	
0.1	$9.760 \cdot 10^{-5}$	1.999	$1.084 \cdot 10^{-6}$	2.000	$1.533 \cdot 10^{-6}$	2.000
0.2	$3.902 \cdot 10^{-4}$	1.999	$4.335 \cdot 10^{-5}$	1.999	$6.130 \cdot 10^{-6}$	1.999
0.25	$6.096 \cdot 10^{-4}$	1.999	$6.771 \cdot 10^{-5}$	1.999	$9.574 \cdot 10^{-6}$	1.999
0.5	$2.432 \cdot 10^{-3}$	1.996	$2.702 \cdot 10^{-4}$	1.996	$3.819 \cdot 10^{-5}$	1.996

TABLE I: Error norms and estimated convergence rates for waves in a piezoelectric material, with $h = 10\Delta t$.

VII. A SURFACE ACOUSTIC WAVE APPLICATION

In order to show that our suggested numerical model may be applied to real-world phenomena, we apply it to a problem in quantum electronics, specifically in acoustic charge transport. We simulate a SAW propagating through a nano-scale substrate of GaAs. SAWs are particular solutions of Eqs. (9) - (12) such that they propagate without decay on the surface of a material but decay exponentially into the bulk. The solutions typically have the form,

$$\begin{aligned} u_i &= \sum_j U_{i,j} e^{-kq_j z} e^{i(kx - \omega t)}, \\ \phi &= \sum_j \Phi_j e^{-kq_j z} e^{i(kx - \omega t)}, \end{aligned} \quad (38)$$

assuming x is the direction of propagation, z is the direction into the bulk ($z \rightarrow -\infty$), and the decay constants q_j , may be complex, allowing for oscillatory decay (in an exponential envelope) into the bulk as is the case for GaAs [30]. The $U_{i,j}$ and Φ_j are constant amplitudes, and k is a wavenumber. It is a straightforward mathematical procedure to determine the decay constants and wave velocity [18]. However, we are interested in the more complicated dynamics taking place when an obstacle in the form of a charged metallic gate is placed on the surface.

In acoustic charge transport, the time-varying electric potential accompanying the SAW is used to transport electrons which are trapped in the minima of the waves. To perform further manipulation on these electrons, for example, to remove some from a minimum, external electric fields must be applied, and this is achieved by applying voltages to metallic gates placed on the surface. In general, the gates have different electrical and mechanical properties to the bulk piezoelectric material and so we may expect to see interesting effects if for example a SAW is passed through the compound structure. Here, we perform three simulations where we pass a SAW through a piece of GaAs. The first will be a bare SAW, as a check to see we do excite the required modes. The following two will have a metallic gate of contrasting mechanical properties to GaAs with a static voltage applied on it. In the first of these, we decouple the mechanical motion from the electric field (while keeping the electric field coupled to the mechanical motion). In the second we allow the full mutual coupling between the electrical and mechanical fields to take place. The dimensions of the gate are $600 \text{ nm} \times 400 \text{ nm} \times 200 \text{ nm}$. To magnify the effect of the compound material structure we use a fictitious material for the gate, similar in crystal structure to GaAs, but with the elastic constants and mass density changed by one order of magnitude. Moreover, we apply a relatively large voltage of 1.5 V so that the coupling of the mechanical displacement to the electric field is evident.

In the numerical simulations we have implemented 8-noded hexahedral brick elements with $2 \times 2 \times 2$ Gauss-Legendre integration. The spacing along the direction of the SAW propagation - Δx is chosen to be 100 nm. The time integration parameter Δt is 1.25×10^{-2} ns.

A. Experiments with surface acoustic waves

In realistic SAW-based devices, bulk waves and SAWs are excited by the application of a microwave signal to an interdigitated transducer. The waves propagate outward from the source, with bulk waves dissipating energy into the bulk and surface acoustic waves travelling through the free surface. In acoustoelectric charge transport experiments, the quantum devices are located several thousand microns away from the source where one would expect to see only surface acoustic waves. To simulate the entire system would therefore require vast computational resources (the wavelength of a SAW is one micron and approximately ten nodes would be required across one wavelength for a satisfactory description). Instead we describe a system of boundary conditions which excite acoustic waves with SAWs dominating over the bulk

waves within a few microns of the source.

1. Excitation of SAWs.

We point out that to be consistent with the formulation presented in the previous sections and hence acoustoelectric charge transport experiments, in our simulations the SAW travels along the crystal positive $[011]$ axis, with the positive z axis aligned with the crystal positive $[100]$ axis.

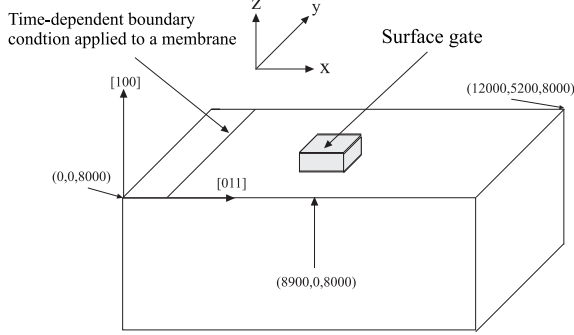


FIG. 2: A schematic diagram of the experimental setup for simulating SAWs. The gate is centered at $(8.9 \cdot 10^3 \text{ nm}, 2.6 \cdot 10^3 \text{ nm})$

In order to excite the SAW modes, we apply a time-dependent Dirichlet boundary condition to the z component of the displacement field on a small region on the grid. This can be expressed as

$$\begin{aligned} u_x = u_y = 0, \quad u_z = A \sin(2\pi ft), \\ x_0 \leq x \leq x_1, \quad z = 8000 \text{ nm}. \end{aligned} \quad (39)$$

The thickness of the membrane is defined as $x_1 - x_0 = 100 \text{ nm}$. To reduce diffraction effects from the surfaces - $y = 0 \text{ nm}$ and $y = 5200 \text{ nm}$ we have forced $u_y = 0$ on those faces. The frequency f used is 2.7 GHz and the amplitude A is chosen so that the SAW amplitude is approximately 20 mV at a depth of 100 nm . Traction free boundary conditions for the mechanical equations and zero normal electrical displacements are implemented at the surfaces. We found this system of boundary conditions to be a particularly efficient means of generating coherent SAWs. The setup is shown in Fig. 2.

Figure 3 is a result of a simulation showing the $\frac{\pi}{2}$ phase difference between the x and z components of the displacement vector, and the larger z amplitude, suggesting elliptical polarization in the sagittal plane. Figures 4(a) and 4(b) show two-dimensional slices, in perpendicular planes, of the full three-dimensional solutions. The first shows the non-decaying nature of these waves along the propagation direction. The SAW wavelength can be seen to be approximately 1000 nm and its velocity is computed to be approximately $2700 \pm 20 \text{ ms}^{-1}$, which is in

good agreement with analytical calculations for the wave velocity. The second figure shows the surface nature of these waves; the greatest amplitude is near the surface and there is no observable decay in the direction of propagation but they decay exponentially into the bulk. On the far left of each image (close to where the boundary condition is applied), bulk waves may be observed but as the waves propagate towards the right, they dissipate all their energy into the bulk and the only remaining waves are the surface waves. Figure 5 shows the SAW amplitude as a function of depth. We see that the amplitude undergoes oscillatory (complex exponential) decay into the bulk and is negligible a few microns below the surface, again in good agreement with analytical expressions derivable from Eq. (38) [30].

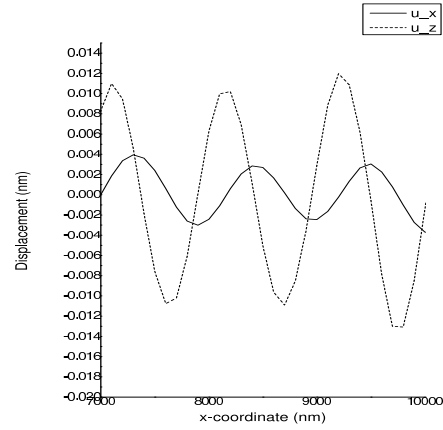


FIG. 3: The relative amplitudes and phases of the displacements u_x and u_z , parallel and perpendicular respectively, to the SAW propagation.

2. The effect of the compound mechanical structure.

Figure 6(a) shows the magnitude of the displacement field as the SAW moving from the left of the figure to the right, passes through the gate when the mechanical motion is decoupled from the electric field. The gate is centered at $(8.9 \cdot 10^3 \text{ nm}, 2.6 \cdot 10^3 \text{ nm})$. We observe a peak to the left of the gate (due to a reflection) and a trough (due to damping of the wave) to the right. We also just barely see vibrations moving away from the gate along the y direction. Since in this simulation, the mechanical motion is independent of the electric fields, this damping is due purely to the presence of a mechanical structure on the surface. The damping of the mechanical amplitude may be large enough to affect the electric potential. In this simulation, the electric potential is not affected significantly as shown in Fig. 6(b). The central blur is the electric potential due to the gate. The SAW peak

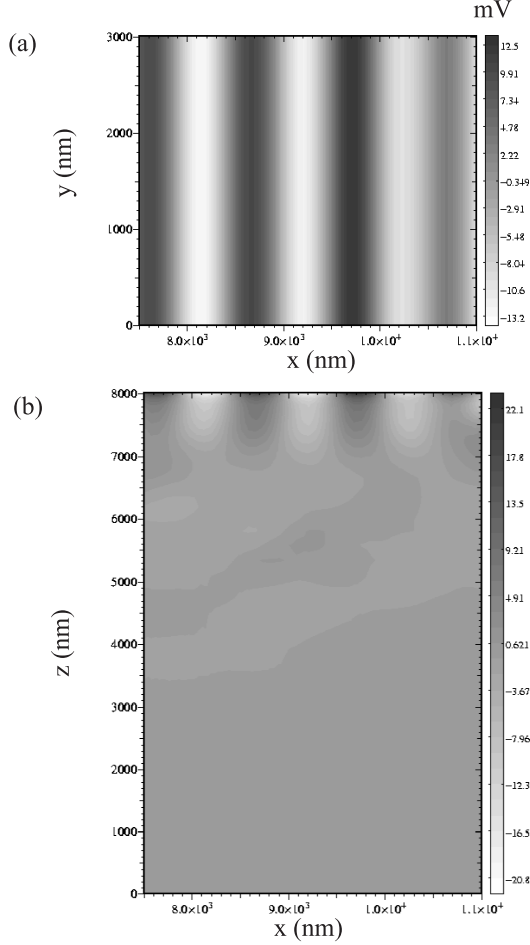


FIG. 4: (a) Plane waves of the electric potential, 100 nm below the surface, at time 1.6 ns. (b) Surface nature of the electric potential, at time 1.6 ns. The SAWs have a significant amplitude between $z = 8000$ nm and $z = 7000$ nm and have a significantly reduced amplitude below $z = 7000$ nm

emerging from the gate has been damped in the central region.

3. The effect of electromechanical coupling.

Figure 7(a) shows the magnitude of the displacement field, at time 2 ns, as the SAW passes through the gate, in the case where mutual coupling between the electric and mechanical fields is allowed. As in the decoupled case, we observe a peak to the left of the gate (due to reflection of the wave) and a trough (due to damping of the wave) to the right. Again, we also see vibrations moving away from the gate along the y direction. Comparing Figs. 6(a) and 7(a), we see that there is additional mechanical deformation throughout the material due to the presence of a charged metallic gate. Also, the scale of Fig. 7(a) is shifted up compared to that of Fig. 6(a). By

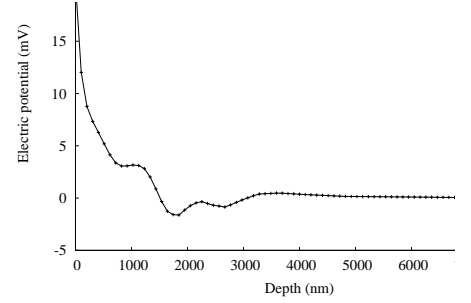


FIG. 5: A typical curve of the electric potential as a function of depth into the bulk. The precise shape of the curve clearly depends on the exact time and spatial coordinate the data was taken as the amplitude of the SAW varies from -20 mV to $+20$ mV. However, all such curves have the oscillatory decay into the bulk becoming negligible within a few microns.

looking at the displacement field at time 0 i.e. before the arrival of the SAW, we can see the displacement resulting from the applied electric field. This is shown in Fig. 7(b).

VIII. SUMMARY AND CONCLUDING REMARKS

Our aim with this paper is to suggest a computationally fast method for simulating SAWs in piezoelectric devices where stress, deformation, and a quasi-static electric field are fully coupled. The basic idea of the numerical scheme is to use a finite difference approximation in time that decouples the elasticity and the electric field problems such that these can be solved in sequence at each time level. This decoupling can also be explored in computer implementations, because independent solvers for anisotropic elasticity problems and Poisson problems can be joined together. We showed in particular how object-oriented programming techniques can realize such couplings in a very convenient way.

Through numerical experiments in a physically one-dimensional wave propagation problem we have verified that the three-dimensional code reproduces the expected quadratic convergence in space and time if linear or trilinear elements are used. Finally, we have applied the proposed numerical methodology to real SAW phenomena in a device with complicated geometry. We have described a system of boundary conditions which are capable of exciting SAW modes in a small computational domain. We have performed simulations where we have demonstrated the effects on the SAW of a charged metallic gate. The results indicate that the method is capable of predicting the expected complex elasto-electric dynamics in such a device.

The methodology could easily be applied to simulate SAWs through devices such as GaAs/AlGaAs heterostructures with more complicated surface gate geome-

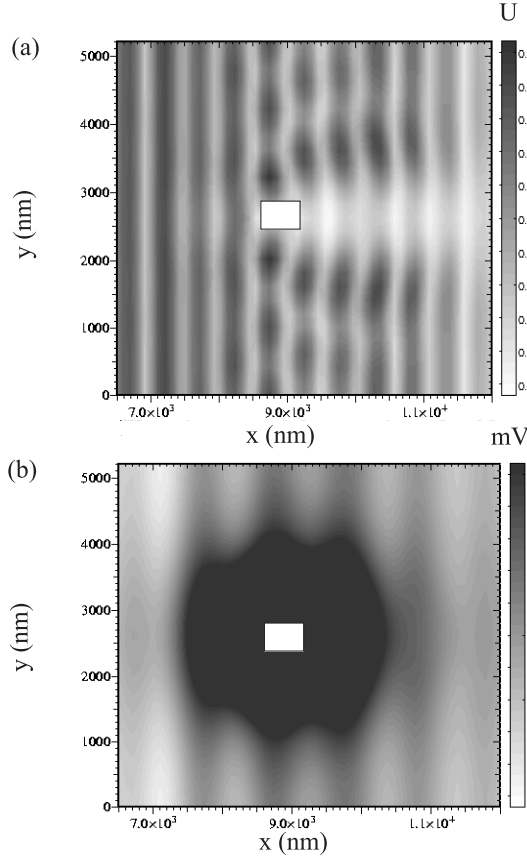


FIG. 6: (a) The magnitude of the displacement field $U = \sqrt{u_r u_r}$, at time 2 ns, as the SAW moving from left to right, passes through the gate centered at $(8.9 \cdot 10^3 \text{ nm}, 2.6 \cdot 10^3 \text{ nm})$ and shown by a white square. The mechanical motion is decoupled from the electric field. (b) The total electric potential, at time 2 ns, as the SAW passes through the gate when the mechanical motion is decoupled from the electric field. The scale has been restricted so that the SAW potential is visible. The central blur, which is due to the large external potential has the value of 1.5 V at its center. The white square shows the position of the gate.

tries.

The principal limitation of the equation splitting is a stability criterion on the time step length. Implicit methods may remove time step restrictions, but at a cost of the need to solve large coupled linear systems at each time level. The computer implementation is also more involved and requires a special-purpose solution rather than just joining two well-tested equation components. However, for wave propagation problems one usually needs a fine mesh and a small time step to resolve the waves, typically leading to $h/\Delta t = \text{const}$, which is in accordance with the stability criterion. Explicit time stepping approaches are therefore highly relevant and allow efficient algorithms and implementations.

Forthcoming numerical work will focus on domain decomposition methods for parallelizing the solver and

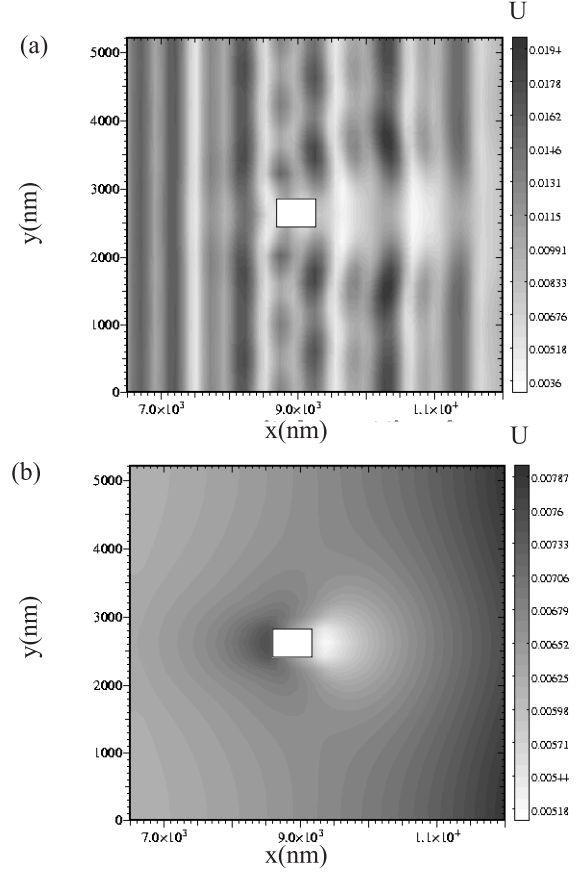


FIG. 7: (a) The magnitude of the displacement field $U = \sqrt{u_r u_r}$, at time 2 ns, as the SAW moving from left to right, passes through the gate centered at $(8.9 \cdot 10^3 \text{ nm}, 2.6 \cdot 10^3 \text{ nm})$ and shown by a white square, when full coupling between electric and mechanical fields is allowed. (b) The magnitude of the displacement field $U = \sqrt{u_r u_r}$, at time 0, demonstrating the mechanical strains caused purely by the gate with a 1.5 V applied voltage centered at $(8.9 \cdot 10^3 \text{ nm}, 2.6 \cdot 10^3 \text{ nm})$ and shown by a white square, when full coupling between electric and mechanical fields are allowed.

thereby enable simulation of large-scale SAW problems. The described time stepping approach and associated equation splitting are particularly well suited for parallel computing, because the elasticity problem can be made “perfectly parallel”, and very efficient parallelization strategies exist for the Poisson equation.

IX. ACKNOWLEDGEMENTS

We thank X. Cai and A. M. Bruaset of Simula Research Laboratory for providing assistance in the programming and debugging of the code, and M. Kataoka of the Cavendish Laboratory for useful discussions. We also acknowledge the Cambridge-MIT Institute, Darwin College Cambridge, and the Simula Research Laboratory

for financial support.

-
- [1] R. Lerch. IEEE Trans. Ultrasonics, Ferroelectrics and Frequency Control, **37**, 233, (1990).
 - [2] A. Benjeddou. Comput. Struct. A, **8**, 347, (2000).
 - [3] S. K. Ha, C. Keilers, and F. K. Chang. AIAA J., **30**, 772, (1992).
 - [4] D. A. Saravanos and P. R. Heyliger. Applied Mechanics Reviews, **52**, 305, (1999).
 - [5] S. V. Gopinathan, V. V. Varadan, and V. K. Varadan. Smart Materials and Structures, **9**, 24, (2000).
 - [6] J. Makerle. Smart materials and structures: FEM and BEM simulations - a bibliography. Finite Elements in Analysis and Design, **37**, 71, (2001).
 - [7] L. Ramdas Ram-Mohan. *Finite Element and Boundary Element Applications in Quantum Mechanics*. Oxford University Press, 1st edition, (2002).
 - [8] A. Wixforth, J. P. Kotthaus, and G. Weimann. Phys. Rev. Lett., **56**, 2104, (1986).
 - [9] J. M. Shilton, V. I. Talyanskii, M. Pepper, J. E. F. Frost, C. J. B. Ford, C. G. Smith, and G. A. C. Jones. J. Phys. Condens. Matter, **8**, 531, (1996).
 - [10] C. H. W. Barnes, J. M. Shilton, and A. M. Robinson. Phys. Rev. B, **62**, 8410, (2000).
 - [11] A. M. Robinson and C. H. W. Barnes. Phil. Trans. R. Soc. Lond., **A 361**, 1487, (2003).
 - [12] A. Bertoni, P. Bordone, R. Brunetti, C. Jacobini, and S. Reggiani. Phys. Rev. Lett., **84**, 5912, (2000).
 - [13] P. Bordone, A. Bertoni, M. Rosini, S. Reggiani, and C. Jacobini. Semicond. Sci. Tech., **19**, (2004).
 - [14] C. L. Foden, V. I. Talyanskii, G. J. Milburn, M. L. Leadbeater, and M. Pepper. Phys. Rev. A, **62**, 11803, (2000).
 - [15] J. Ebbecke, N. E. Fletcher, T. J. B. M. Janssen, F. J. Ahlers, M. Pepper, H. E. Beere and D. A. Ritchie, Phys. Lett. **84**, 4319 (2004).
 - [16] F. Alsina, P. V. Santos, H. P. Schönherr, R. Nötzel and K. H. Ploog, Phys. Rev. B **67**, 161305, (2003).
 - [17] T. Sogawa, P. V. Santos, S. K. Zhang, S. Eshlaghi, A. D. Wieck and K. H. Ploog, Phys. Rev. Lett. **87**, 276601, (2003).
 - [18] H. Matthews. Surface Wave Filters. John Wiley, 1st edition, (1977).
 - [19] J. J. Campbell and W. R. Jones. IEEE Trans. Sonics and Ultrasonics, SU15 No. **4**, 209, (1968).
 - [20] G. R. Aizin and G. Gumbs. Phys. Rev. B, **58**, 10589, (1998).
 - [21] G. Gumbs and G. R. Aizin. Phys. Rev. B, **60**, 954, (1999).
 - [22] A. Preumont. Vibration Control of Active Structures - An Introduction. Kluwer Academic Publishers, (1997).
 - [23] H. P. Langtangen. *Computational Partial Differential Equations - Numerical Methods and Diffpack Programming*. Text in Computational Science and Engineering, vol 1. Springer, 2nd edition, (2003).
 - [24] O. Zienkiewicz. The Finite Element Method. McGraw-Hill, 4th edition, (1994).
 - [25] A. Iserles, *A first course in the numerical analysis of differential equations*, Cambridge University Press, (1995).
 - [26] H. P. Langtangen. International Journal of Numerical Methods in Fluids, **10**, 213, (1989).
 - [27] R. D. Cook, D. S. Malkus, and M. E. Plesha. Concepts and Applications of Finite Element Analysis. Wiley, 3rd edition, (1989).
 - [28] H. P. Langtangen and O. Munthe. ACM Transactions on Mathematical Software, **27**, 1, March (2001).
 - [29] O. Munthe and H. P. Langtangen. Computer Methods in Applied Mechanics and Engineering, **190**, 865, (2000).
 - [30] S. H. Simon, Phys. Rev. B **54**, 13878 (1996).